International Journal of Fracture (2005) 136:1–36
DOI 10.1007/s10704-005-3934-7

On the path independency of the point-wise J integral in three-dimensions

NETTA OMER and ZOHAR YOSIBASH*
Pearlstone Center for Aeronautical Engineering Studies, Department of Mechanical Engineering, Ben-Gurion University of the Negev, Beer-Sheva 84105, Israel
Author for correspondence. (E-mail: nettao/zohary@bgu.ac.il)

Received 5 January 2005; accepted in revised form 10 October 2005

Abstract. The asymptotic solution in the vicinity of a crack front in a three-dimensional (3-D) elastic domain is provided explicitly following the general framework in M. Costabel, M. Dauge and Z. Yosibash, 2004, *SIAM Journal of Mathematical Analysis*, **35**(5), 1177–1202. Using it, we show analytically for several fully 3-D displacement fields (which are neither plane strain nor plane stress) that the pointwise path-area J_{X_1}-integral in 3-D is path-independent. We then demonstrate by numerical examples, employing p-finite element methods, that good numerical approximations of the path-area J_{X_1}-integral may be achieved which indeed show path independency. We also show that computation of the path part of the J_{X_1} on a plane perpendicular to the crack front is path dependent. However, one may still use this path integral computed at several radii, followed by the application of Richardson's extrapolation technique (as $R \to 0$) to obtain a good estimate for J_{X_1}-integral.

Key words: Edge stress intensity functions, high order finite elements, J-integral.

1. Introduction

The most important parameters in linear elastic fracture mechanics (LEFM) are the stress intensity factors (SIFs), which are associated directly or indirectly with fracture criteria and crack propagation. The most common extraction method for these parameters in two-dimensional (2-D) domains relay on a path independent integral, called the J-integral, surrounding the crack tip. The J-integral was presented for two-dimensional domains by Cherepanov (1967) and Rice (1968). A vast amount of research has focused in the past on extending its applicability to cracks in three-dimensional (3-D) domains, however as will be discussed in the sequel, the extension requires some assumptions which restrict its generality and applicability.

We herein present explicit representation of the displacements field in the vicinity of a three-dimensional crack edge in isotropic elastic domains. Both traction free and clamped boundary conditions are considered on the crack faces, and general displacement fields are derived in the vicinity of the crack edge (without any restriction, as plane strain or plane stress conditions, applied). Using the explicit solutions we show that the past known extensions of the J-integral to three-dimensions yield a pointwise path-area *independent* integral. Several publications in the past show that the pointwise path-area J-integral is path-area independent for the special cases of plane-strain/stress conditions, as well as for a path which tends to zero. Nevertheless, for a path surrounding the crack edge at a finite distance, under a more general

3-D displacement field, such evidence is not available. Herein we extend the path-area independency of this 3-D pointwise J-integral to more general cases involving both clamped and traction free crack faces, without the need of assuming plane-strain or plane-stress assumptions.

1.1. The path independent J integral for 2-D domains

The J-integral was presented by Cherepanov (1967) and by Rice (1968), for two-dimensional domains containing cracks. Consider a 2-D crack along the X_1 axis as shown in Figure 1. To distinguish between 2-D and 3-D quantities, Latin indices range from 1 to 2, and i, j and k indices range from 1 to 3. Herein we use the Einstein summation notation, where 2 repeated indices represent summation. The well known path independent J-integral in 2-D domain is given by:

$$J = \int_\Gamma (W\,\mathrm{d}X_2 - \boldsymbol{T}\cdot\partial_1\boldsymbol{U}\,\mathrm{d}S) \tag{1}$$

where W is the strain-energy density ($W = \int_0^\varepsilon \sigma_{\beta\gamma}\mathrm{d}\varepsilon_{\beta\gamma}$) which equals $\frac{1}{2}\sigma_{\beta\gamma}\varepsilon_{\beta\gamma}$ in linear elasticity, $\varepsilon_{\beta\gamma} = \frac{1}{2}(\partial_\beta U_\gamma + \partial_\gamma U_\beta)$ is the infinitesimal strain tensor, $\boldsymbol{U} = \{U_1, U_2, U_3\}^T$ is the displacement vector, $\partial_\beta = \frac{\partial}{\partial X_\beta}$ and $\boldsymbol{T}$ ($T_\beta = \sigma_{\gamma\beta}n_\gamma$) is the traction vector defined according to the outward normal to the path Γ, and Γ is any path initiating at one face and terminating on the other face of the crack, surrounding the crack tip as illustrated in Figure 1. The J-integral was proved to be path independent in 2-D domains. The proof is presented for completeness in Appendix A. The property of path-independency of the J-integral combined with the fact that it equals to the strain energy release rate $\mathcal{G}$ in linear elastic bodies, enables one to compute the stress intensity factors K_I and K_{II}:

$$J = \mathcal{G} = \frac{K_I^2 + K_{II}^2}{E^*} \qquad E^* = \begin{cases} E & \text{for plane stress,} \\ \frac{E}{1-\nu^2} & \text{for plane strain.} \end{cases} \tag{2}$$

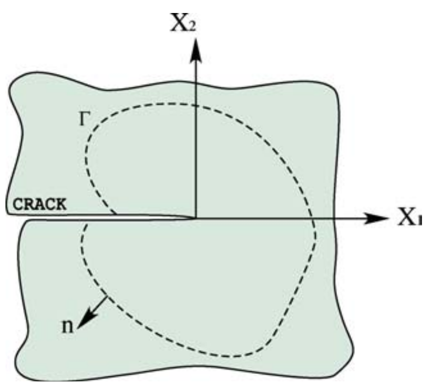

Figure 1. Two dimensional domain with a crack. Γ is any curve surrounding the crack.

1.2. The point-wise J_{X_1}-integral for three-dimensional domains

Extension of the J-integral to 3-D linear elastic domains containing a crack has been approached by two different methods. The first extends the original 2-D J-integral to a 3-D integral as shown by Chiarelli and Frediani (1993) and Huber et al. (1993). The second method is by using the virtual crack extension method for a 3-D domain containing a crack as obtained by Shih et al. (1986). They considered a small increment along the crack tip, δs, in the vicinity of the singular point, s. They allow a virtual crack to advance in the direction normal to the crack front. As a result a volume integral is obtained. When the increment of crack length tends to zero ($\delta s \to 0$) the integral becomes identical to the integral obtained by Huber et al. (1993). Finite element methods are used to compute the volume integral and an example of an axisymmetric crack is presented. Both methods lead to the same formulation providing the point-wise value of the J-integral at a given point s along the crack front:

$$J_{X_1}(s) = \int_{\Gamma} \left(W n_1 - \sigma_{ij} n_j \cdot \partial_1 U_i \right) \mathrm{d}s - \int_{A(\Gamma)} \partial_3 \left(\sigma_{i3} \partial_1 U_i \right) \mathrm{d}A(\Gamma), \tag{3}$$

where s is a point along the crack front, W in this case equals $\frac{1}{2}\sigma_{ij}\varepsilon_{ij}$ and X_1 is a Cartesian coordinate normal to the crack front at point s, as illustrated in Figure 2. It is important to note that the path-area independency in Shih et al. (1986), Chiarelli and Frediani (1993) and Huber et al. (1993) is obtained under the assumption of plane-strain/stress, or at the limit when $A(\Gamma) \to 0$.

The J_{X_1} contains two integrals: the first is a path integral and the second is an area integral. Both the path Γ and the area (enclosed by the path Γ) lay in X_1–X_2 plane which is perpendicular to the crack front. In computing $J_{X_1}(s)$, the *derivatives* of stresses, strains and displacements are required, and when based on numerical approximations their values in the vicinity of a singular point is poor. Therefore the computation of the area integral with a reasonable numerical accuracy is not an easy task.

Rigby and Aliabadi (1998) have shown that *under plane stress or plane strain* assumption, the path-area integral, $J_{X_1}(s)$ is path-area independent. They proved that for any selection of path Γ the $J_{X_1}(s)$ integral has the same value. The $J_{X_1}(s)$-integral was also addressed by Gosz et al. (1998). Although the volume integral was presented, the authors use either plane stress or plane strain assumptions in order to calculate

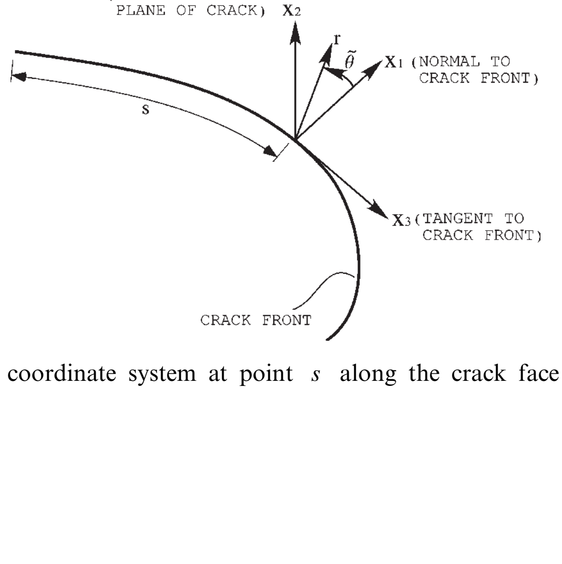

Figure 2. The local coordinate system at point s along the crack face in a 3-D domain.

$J_{X_1}(s)$ and therefore the volume integral is reduced to an area integral. The method is applicable to bimaterial cracks when only K_I and K_{II} are considered. Chiarelli and Frediani also used numerical methods for the computation of $J_{X_1}(s)$. Their method involves coordinates change according to the selected point s along the crack front. The stress and displacement components are extracted from the finite element solution where the derivatives (as $\partial_1 U_2$ and $\partial_1 U_3$) are obtained by differentiating the shape functions. Gauss quadrature integration is used for calculation of the path and area integrals of $J_{X_1}(s)$.

The area integral in $J_{X_1}(s)$ was addressed also by Eriksson (2000). He demonstrates that the area integral can be simplified in some crack geometries by changing the coordinate system of the integration according to the geometry of the crack. Moreover, Eriksson shows that there are four geometry conditions in which the area integral vanishes. The first two conditions are related with the geometry of the crack and the other two terms are related with the selection of coordinate system for integration of $J_{X_1}(s)$.

Beyond the numerical difficulties associated with the need to use numerical values and derivatives close to the singular points, many publications in the past 10 years apply the restriction of plane strain or plane stress when computing the $J_{X_1}(s)$-integral. However, in a general 3-D domain, even when a simple straight crack front is present, neither a plane strain nor a plane stress situation exists, and in this case we show evidence that the $J_{X_1}(s)$-integral is still path independent if both the path *and* the area integral are computed. A remedy to the need of computing the area integral is by using the path integral alone (as in a 2-D case) at different circles with decreasing radii, followed by Richardson's extrapolation as the radius tends to zero.

We provide in Section 2 the asymptotic solution of the displacements in the vicinity of a 3-D cracked edge – both traction free and clamped boundary conditions on crack faces are considered. We chose six problems with analytical solutions (two of which are plane-strain) to be used in Section 3 to examine the $J_{X_1}(s)$-integral. In Section 3 we show that for all six problems of interest $J_{X_1}(s)$ is path independent and provide also numerical results illustrating the path-independency. One may compute only the path-part of the integral (as in 2-D domains) at decreasing radii in conjunction with Richardson's extrapolation for an accurate determination of $J_{X_1}(s)$. Finally, we consider a common problem of engineering interest, the compact tension specimen (CTS), and apply the suggested methods to compute $J_{X_1}(s)$ at two points along it's crack edge.

2. The elastic solution in the vicinity of the crack front (edge)

In three-dimensional domains three different functional representation of the singular solutions to the Navier–Lamé equations exist, depending whether one is interested in the vicinity of an edge, a vertex or the intersection of the edge with the vertex (see Figure 3). In this work we consider the solution in the vicinity of an edge only (which is denoted by $\mathcal{E}$). Our point of departure is the functional representation of the elastic solution (displacements or stresses) in the vicinity of the crack front (edge), which may be characterized by an infinite number of eigen-pairs.

Although the asymptotic expansion for the two-dimensional stress fields in the vicinity of a singular point is well known, in reality three-dimensional domains are

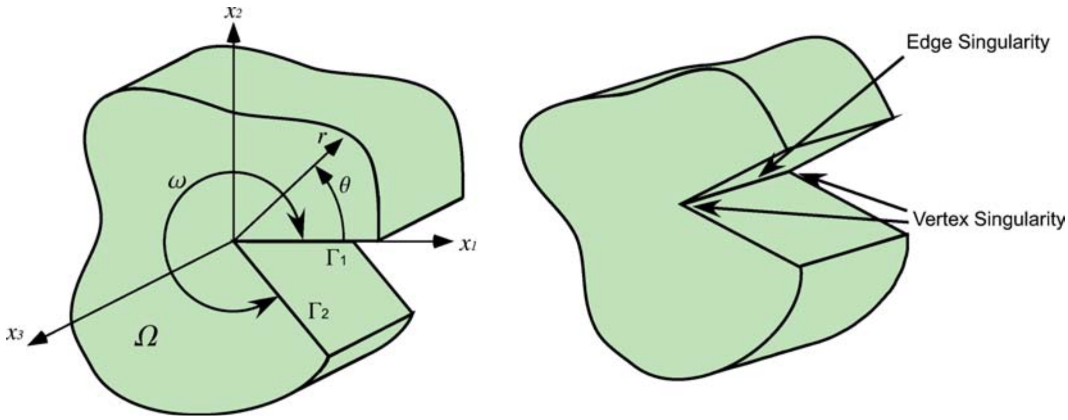

Figure 3. (a) Schematic 3-D domain, Ω; (b) edge and vertex singularities in 3-D domain.

present. Therefore a refined analysis for three-dimensional solutions in the vicinity of an edge is required. Hartranft and Sih (1967) are the first (to the best of our knowledge) to address the elastic solution in the vicinity of a three-dimensional crack front. However, their solution has not been widely used due to its complexity and lack of explicit representation. Leblond and Torlai (1992) present the solution of the displacements and stresses in the vicinity of a straight and curved crack front in 3-D domains, however, the assumption of plane strain is adopted, so that the fully 3-D asymptotic solution is not provided. Nevertheless, using the plane-strain asymptotic solution, the expansion for curved crack fronts is derived, containing higher order terms and an explicit dependency of the "stress intensity factors" on the crack front coordinate. Lately, a simplified algorithm which explicitly provides the functional representation of the elastic solution (eigen-pairs computation) in a general setting for elliptic problems is provided in Costabel et al. (2004). An explicit use for the algorithm is given in Omer et al. (2004) where the explicit solution for a scalar elliptic problem is provided. In this section the asymptotic solution (the displacements) in the vicinity of a 3-D cracked edge is derived which is subsequently used to show that the pointwise path-area $J_{X_1}(s)$-integral is path independent.

2.1. Differential equations for 3-D eigen-pairs

Consider a 3-D domain Ω with a solid angle ω, created by the intersection of two flat surfaces, as shown in Figure 3. In the case $\omega=2\pi$, a cracked domain is obtained. We denote the flat surfaces by Γ_1 and Γ_2.

Remark 1. For mathematical convenience, the coordinate system presented in this chapter is denoted by x_1, x_2, x_3, so that the x_1 axis lies along crack's faces. This notation is different compared to the coordinate system, X_1, X_2, X_3, used for the definition of quantities in the $J_{X_1}(s)$-integral. The two systems are connected by the relationships $x_1=-X_1$ and $x_3=-X_3$. The displacements in the $\boldsymbol{X}$ system will be denoted by $\boldsymbol{U}$, and in the $\boldsymbol{x}$ system by $\boldsymbol{u}$. In order to compute the $J_{X_1}(s)$-integral the displacements, after being derived, will be transferred into the X_1, X_2, X_3 system, as will be presented in Appendix B. The polar coordinate system related with cartesian system $\boldsymbol{X}$ is, $r, \tilde{\theta}, X_3$, where the polar coordinate system related with $\boldsymbol{x}$ is, r, θ, x_3.

For simplicity of presentation assume that the domain Ω contains only one straight edge $\mathcal{E}$, and is generated by the product $\Omega = G \times I$ where I is an interval $[-x_3, x_3]$, and G is a plane bounded sector of opening ω. The coordinate system is chosen so that G coincides with the (x_1, x_2) plane and I is along x_3. We denote the coordinates (x_1, x_2, x_3) by $\boldsymbol{x}$. Let (r, θ) be polar coordinates centered at the vertex of G. The *edge* $\mathcal{E}$ of interest is the set $\{\boldsymbol{x} \in \mathbb{R}^3 \,|\, r = 0,\ x_3 \in I\}$. To distinguish between the displacements vector in Cartesian or polar coordinates, we denote the later by $\tilde{\boldsymbol{u}} = \{u_r, u_\theta, u_{x_3}\}^T$ and use either of them when more convenient.

Remark 2. The methods presented herein are restricted to geometries where the edges are straight lines and the angle ω is fixed along x_3.

The exact solution of the Navier–Lamè (N–L) system of equations, $\mathcal{L}(\tilde{\boldsymbol{u}}) = 0$, ($\mathcal{L}$ denotes the N–L operator), in the neighborhood of the edge $\mathcal{E}$ is obtained by splitting the operator $\mathcal{L}$ into three parts (see Dauge, 1988; Costabel and Dauge, 1993):

$$\mathcal{L} = [M_0(\partial_r, \partial_\theta)] + [M_1(\partial_r, \partial_\theta)]\partial_3 + [M_2]\partial_3^2 \tag{4}$$

where $[M_i]$ are 3×3 matrix operators (presented in explicit form in the sequel). The splitting allows the consideration of a solution $\tilde{\boldsymbol{u}}$ of the form:

$$\tilde{\boldsymbol{u}} = \sum_{j \geqslant 0} \partial_3^j A(x_3) \boldsymbol{\Phi}_j(r, \theta) \tag{5}$$

herein $\partial_3^j \equiv \dfrac{\partial^j}{\partial x_3}$. The N–L system in view of (5) becomes:

$$\sum_{j \geqslant 0} \partial_3^j A(x_3)[M_0]\boldsymbol{\Phi}_j + \sum_{j \geqslant 0} \partial_3^{j+1} A(x_3)[M_1]\boldsymbol{\Phi}_j + \sum_{j \geqslant 0} \partial_3^{j+2} A(x_3)[M_2]\boldsymbol{\Phi}_j = 0 \tag{6}$$

and after rearranging:

$$\begin{aligned} & A(x_3)[M_0]\boldsymbol{\Phi}_0 + \partial_3 A(x_3)([M_0]\boldsymbol{\Phi}_1 + [M_1]\boldsymbol{\Phi}_0) + \\ & \quad + \sum_{j \geqslant 0} \partial_3^{j+2} A(x_3) \left([M_0]\boldsymbol{\Phi}_{j+2} + [M_1]\boldsymbol{\Phi}_{j+1} + [M_2]\boldsymbol{\Phi}_j\right) = 0. \end{aligned} \tag{7}$$

Equation (7) has to hold for any smooth function $A(x_3)$. Thus, the functions $\boldsymbol{\Phi}_j$ must satisfy the three equations below, each defined on a two-dimensional domain G which is generated by the intersection of a plane perpendicular to the crack edge and the 3-D domain:

$$\begin{cases} [M_0]\boldsymbol{\Phi}_0 = 0 & \\ [M_0]\boldsymbol{\Phi}_1 + [M_1]\boldsymbol{\Phi}_0 = 0 & \qquad (r, \theta) \in G \\ [M_0]\boldsymbol{\Phi}_{j+2} + [M_1]\boldsymbol{\Phi}_{j+1} + [M_2]\boldsymbol{\Phi}_j = 0, \quad j \geqslant 0 & \end{cases} \tag{8}$$

accompanied by either traction free or homogeneous Dirichlet boundary conditions on the two surfaces Γ_1 and Γ_2.

The first partial differential equation in (8) generates the solution $\boldsymbol{\Phi}_0$, denoted *primal singular function*, which is the well known two-dimensional eigen-function of the form:

$$\boldsymbol{\Phi}_0 = r^{\alpha}\varphi_0(\theta), \tag{9}$$

where $\boldsymbol{\Phi}_0$ is the eigen-function associated with the eigen-value α of the degenerate boundary value problem over the 2-D domain G. The second PDE in (8) generates the function $\boldsymbol{\Phi}_1$ which depends on $\boldsymbol{\Phi}_0$ and is of the form:

$$\boldsymbol{\Phi}_1 = r^{\alpha+1}\varphi_1(\theta). \tag{10}$$

The sequence $\boldsymbol{\Phi}_j$ (where $j \geqslant 2$) are the solutions of the third equation of (8). These are of the form:

$$\boldsymbol{\Phi}_j = r^{\alpha+j}\varphi_j(\theta). \tag{11}$$

The $\boldsymbol{\Phi}_j$, where $j > 1$ are called *shadow functions* associated with the primal function $\boldsymbol{\Phi}_0$. There are an infinite number of shadow functions $\boldsymbol{\Phi}_j$ associated with any positive eigen-value α_i, and therefore:

$$\boldsymbol{\Phi}_j^{(\alpha_i)} = r^{\alpha_i+j}\varphi_j^{(\alpha_i)}(\theta) \quad j = 0, 1, \ldots \tag{12}$$

Thus, for each eigen-value α_i, the 3-D solution, in the vicinity of an edge is:

$$\tilde{\boldsymbol{u}}^{(\alpha_i)} = \sum_{j\geqslant 0} \partial_3^j A_i(x_3) r^{\alpha_i+j}\varphi_j^{(\alpha_i)}(\theta) \tag{13}$$

and the overall solution $\tilde{\boldsymbol{u}}$ is:

$$\tilde{\boldsymbol{u}} = \sum_{i\geqslant 1}\sum_{j\geqslant 0} \partial_3^j A_i(x_3) r^{\alpha_i+j}\varphi_j^{(\alpha_i)}(\theta) \tag{14}$$

where $A_i(x_3)$ is the edge stress intensity function (ESIF) associated with the ith eigen-value.

2.2. Boundary conditions for the primal and shadow eigen-functions

We will consider either traction free or clamped (homogeneous Dirichlet) boundary conditions on the two flat surfaces Γ_1 and Γ_2.

2.2.1. *Traction free boundary conditions*

Assuming traction free boundary conditions on Γ_1 and Γ_2 results in:

$$[T](\vec{\tilde{u}})|_{\Gamma_1,\Gamma_2} = \big([T_0](\partial_r, \partial_\theta)\tilde{\boldsymbol{u}} + [T_1](\partial_r, \partial_\theta)\partial_3\tilde{\boldsymbol{u}}\big)|_{\Gamma_1,\Gamma_2} = 0 \tag{15}$$

The operators $[T_0]$ and $[T_1]$ are explicitly provided in (26) in the next sub-section. Inserting (5) in (15) one obtains:

$$\sum_{j\geqslant 0} \partial_3^j A(x_3)[T_0]\boldsymbol{\Phi}_j|_{\Gamma_1,\Gamma_2} + \sum_{j\geqslant 0} \partial_3^{j+1} A(x_3)[T_1]\boldsymbol{\Phi}_j|_{\Gamma_1,\Gamma_2} = 0 \tag{16}$$

and after rearranging:

$$A(x_3)[T_0]\mathbf{\Phi}_0|_{\Gamma_1,\Gamma_2}+\sum_{j\geqslant 0}\partial_3^{j+1}A(x_3)\left([T_0]\mathbf{\Phi}_{j+1}+[T_1]\mathbf{\Phi}_j\right)|_{\Gamma_1,\Gamma_2}=0. \tag{17}$$

Equation (17) has to hold for any smooth function $A(x_3)$ and therefore the boundary conditions for the eigen-functions are:

$$\begin{cases}[T_0]\mathbf{\Phi}_0=0\\ [T_0]\mathbf{\Phi}_{j+1}+[T_1]\mathbf{\Phi}_j=0, \quad j\geqslant 0\end{cases} \quad \text{on} \quad \Gamma_1,\Gamma_2. \tag{18}$$

The first equation in (18) is the boundary conditions for $\mathbf{\Phi}_0$ which is identical to the 2-D problem. The second equation in (18) is the boundary conditions for each $\mathbf{\Phi}_j$ where $j\geqslant 1$.

2.2.2. *Homogeneous dirichlet boundary conditions*
Assuming homogeneous Dirichlet boundary conditions on Γ_1 and Γ_2 results in:

$$\tilde{\boldsymbol{u}}|_{\Gamma_1,\Gamma_2}=\sum_{i\geqslant 1}\sum_{j\geqslant 0}\partial_3^j A_i(x_3)r^{\alpha_i+j}\varphi_j^{(\alpha_i)}(\theta)|_{\Gamma_1,\Gamma_2}=0 \tag{19}$$

and therefore

$$\varphi_j(\theta)=0, \quad j\geqslant 0 \quad \text{on} \quad \Gamma_1,\Gamma_2 \tag{20}$$

2.3. Explicit expressions for eigen-pairs for a crack

Consider a domain Ω in which I is the interval $[-1, 1]$, and G is a plane bounded sector of opening $\omega=2\pi$ defined by $\{r\in(0,1),\ \theta\in(0,\omega)\}$ (the case of a crack), as shown in Figure 4. Although any radius or interval I can be chosen, these simplified numbers have been chosen for simplicity of presentation (we select for example the units of the interval I and the radius r to be [meters]). The edge of interest $\mathcal{E}$ is the set $\{\boldsymbol{x}\in\mathbb{R}^3\,|\,r=0,\ x_3\in I\}$.

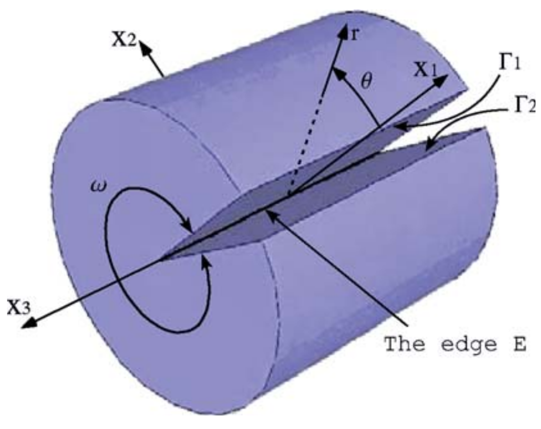

Figure 4. Model domain of interest Ω.

The Navier–Lamé equations (4) in polar coordinates are:

$$(\lambda+2\mu)\partial_r^2 u_r+(\lambda+2\mu)\frac{1}{r}\partial_r u_r-(\lambda+2\mu)\frac{1}{r^2}u_r+\mu\frac{1}{r^2}\partial_\theta^2 u_r+\mu\partial_3^2 u_r$$
$$-(\lambda+3\mu)\frac{1}{r^2}\partial_\theta u_\theta+(\lambda+\mu)\frac{1}{r}\partial_r\partial_\theta u_\theta+(\lambda+\mu)\partial_r\partial_3 u_3=0 \tag{21}$$

$$(\lambda+\mu)\frac{1}{r}\partial_r\partial_\theta u_r+(\lambda+3\mu)\frac{1}{r^2}\partial_\theta u_r+(\lambda+2\mu)\frac{1}{r^2}\partial_\theta^2 u_\theta+\mu\partial_r^2 u_\theta$$
$$+\mu\frac{1}{r}\partial_r u_\theta-\mu\frac{1}{r^2}u_\theta+\mu\partial_3^2 u_\theta+(\lambda+\mu)\frac{1}{r}\partial_3\partial_\theta u_3=0 \tag{22}$$

$$(\lambda+\mu)\partial_r\partial_3 u_r+(\lambda+\mu)\frac{1}{r}\partial_3 u_r+(\lambda+\mu)\frac{1}{r}\partial_3\partial_\theta u_\theta+\mu\partial_r^2 u_3$$
$$+\mu\frac{1}{r}\partial_r u_3+\mu\frac{1}{r^2}\partial_\theta^2 u_3+(\lambda+2\mu)\partial_3^2 u_3=0 \tag{23}$$

with λ, μ being the Lamé constants associated with the engineering material constants E the Young modulus and ν the Poisson ratio. The system (21)–(23) can be expressed as:

$$\mathcal{L}(\tilde{\boldsymbol{u}})=[M_0](\partial_r,\partial_\theta)\tilde{\boldsymbol{u}}+[M_1](\partial_r,\partial_\theta)\partial_3\tilde{\boldsymbol{u}}+[M_2](\partial_r,\partial_\theta)\partial_3^2\tilde{\boldsymbol{u}}=0$$

with:

$$[M_0]=\begin{pmatrix}(\lambda+2\mu)\left(\partial_r^2+\frac{1}{r}\partial_r-\frac{1}{r^2}\right)+\mu\frac{1}{r^2}\partial_\theta^2 & -(\lambda+3\mu)\frac{1}{r^2}\partial_\theta+(\lambda+\mu)\frac{1}{r}\partial_r\partial_\theta & 0\\ (\lambda+\mu)\frac{1}{r}\partial_r\partial_\theta+(\lambda+3\mu)\frac{1}{r^2}\partial_\theta & (\lambda+2\mu)\frac{1}{r^2}\partial_\theta^2+\mu\left(\partial_r^2+\frac{1}{r}\partial_r-\frac{1}{r^2}\right) & 0\\ 0 & 0 & \mu\left(\partial_r^2+\frac{1}{r}\partial_r+\frac{1}{r^2}\partial_\theta^2\right)\end{pmatrix} \tag{24}$$

$$[M_1]=\begin{pmatrix}0 & 0 & (\lambda+\mu)\partial_r\\ 0 & 0 & (\lambda+\mu)\frac{1}{r}\partial_\theta\\ (\lambda+\mu)\left(\partial_r+\frac{1}{r}\right) & (\lambda+\mu)\frac{1}{r}\partial_\theta & 0\end{pmatrix},\quad [M_2]=\begin{pmatrix}\mu & 0 & 0\\ 0 & \mu & 0\\ 0 & 0 & (\lambda+2\mu)\end{pmatrix}. \tag{25}$$

The boundary conditions considered on the crack surface are either traction free or homogeneous Dirichlet. If traction free boundary conditions (15) are considered:

$$\begin{cases}(\sigma_{rr})\,|_{\theta=0,2\pi}=0\\ (\sigma_{r\theta})\,|_{\theta=0,2\pi}=0\\ (\sigma_{r3})\,|_{\theta=0,2\pi}=0\end{cases}\Rightarrow\begin{cases}\left(\mu\left(\frac{1}{r}\partial_\theta u_r+\partial_r u_\theta-\frac{1}{r}u_\theta\right)\right)|_{\theta=0,2\pi}=0\\ \left((\lambda+2\mu)\frac{1}{r}u_r+\lambda\partial_r u_r+(\lambda+2\mu)\frac{1}{r}\partial_\theta u_\theta+\lambda\partial_3 u_3\right)|_{\theta=0,2\pi}=0.\\ \left(\mu\left(\partial_3 u_\theta+\frac{1}{r}\partial_\theta u_3\right)\right)|_{\theta=0,2\pi}=0\end{cases}$$

The boundary conditions are split into two parts as in (15) with:

$$[T_0]=\begin{pmatrix}\mu\frac{1}{r}\partial_\theta & \mu\partial_r-\mu\frac{1}{r} & 0\\ (\lambda+2\mu)\frac{1}{r}+\lambda\partial_r & (\lambda+2\mu)\frac{1}{r}\partial_\theta & 0\\ 0 & 0 & \mu\frac{1}{r}\partial_\theta\end{pmatrix},\quad [T_1]=\begin{pmatrix}0&0&0\\0&0&\lambda\\0&\mu&0\end{pmatrix}. \tag{26}$$

The solution to the first equation in (8) and one of the boundary conditions (the first equation in (18) for traction free boundary conditions and (20) for homogeneous Dirichlet boundary conditions) results in an infinite number of primal eigen-pairs, which are precisely the 2-D eigen-pairs in the vicinity of a crack tip:

$$[M_0]\mathbf{\Phi}_0 = \vec{0}, \quad \left([T_0]\ \mathbf{\Phi}_0|_{0,2\pi} = \vec{0} \text{ or } \mathbf{\Phi}_0|_{0,2\pi} = \vec{0}\right) \Rightarrow \mathbf{\Phi}_0^{(\alpha_i)}, \ \alpha_1 = \alpha_2 = \alpha_3 = 1/2 \cdots \tag{27}$$

With each eigen-value, α_i, there is an associated edge stress intensity function denoted by $A_i(x_3)$.

The shadow function $\mathbf{\Phi}_1$ can then be computed by solving the inhomogeneous PDE in the second equation in (8) with $-[M_1]\mathbf{\Phi}_0$ at the right hand side. The shadow function $\mathbf{\Phi}_2$, and higher order ones are then obtained by the recursive PDE in the third equation in (8).

We further simplify the problem of interest and assume that $A_1(x_3)$ is the only non-zero edge stress intensity function, and is at most a polynomial of degree two (A_1 is associated with mode I loading). In this case $\alpha_1 = \frac{1}{2}$ the exact solution consists of the primal leading function $\mathbf{\Phi}_0^{(\alpha_1)}$ and two shadow functions $\mathbf{\Phi}_1^{(\alpha_1)}, \mathbf{\Phi}_2^{(\alpha_1)}$, having the form:

$$\begin{aligned}
\tilde{\boldsymbol{u}}^{(\alpha_1)} &= A_1(x_3)\mathbf{\Phi}_0^{(\alpha_1)} + \partial_3^1 A_1(x_3)\mathbf{\Phi}_1^{(\alpha_1)} + \partial_3^2 A_1(x_3)\mathbf{\Phi}_2^{(\alpha_1)} \\
&= A_1(x_3) r^{\alpha_1}\varphi_0^{(\alpha_1)} + \partial_3^1 A_1(x_3) r^{\alpha_1+1}\varphi_1^{(\alpha_1)} + \partial_3^2 A_1(x_3) r^{\alpha_1+2}\varphi_2^{(\alpha_1)} \\
&= A_1(x_3) r^{\alpha_1}\begin{pmatrix} u_0(\theta) \\ v_0(\theta) \\ w_0(\theta)\end{pmatrix} + \partial_3^1 A_1(x_3) r^{\alpha_1+1}\begin{pmatrix} u_1(\theta) \\ v_1(\theta) \\ w_1(\theta)\end{pmatrix} + \partial_3^2 A_1(x_3) r^{\alpha_1+2}\begin{pmatrix} u_2(\theta) \\ v_2(\theta) \\ w_2(\theta)\end{pmatrix}.
\end{aligned} \tag{28}$$

We provide now the explicit expressions for the functions $u_0, v_0, \ldots, w_2$, thus, for the traction free boundary conditions the displacements in the vicinity of the crack edge are:

$$\begin{aligned}
\tilde{\boldsymbol{u}}^{(\alpha_1)} &= A_1(x_3) r^{\frac{1}{2}}\begin{pmatrix} (Q_1-1)\sin\left(\frac{1}{2}\theta\right) + \sin\left(\frac{3}{2}\theta\right) \\ (Q_1+1)\cos\left(\frac{1}{2}\theta\right) + \cos\left(\frac{3}{2}\theta\right) \\ 0 \end{pmatrix} \\
&\quad + \partial_3^1 A_1(x_3) r^{\frac{3}{2}}\begin{pmatrix} 0 \\ 0 \\ -2\sin\left(\frac{1}{2}\theta\right) - \frac{2}{3}(Q_1+1)\sin\left(\frac{3}{2}\theta\right)\end{pmatrix} \\
&\quad + \partial_3^2 A_1(x_3) r^{\frac{5}{2}}\begin{pmatrix} Q_2\sin\left(\frac{1}{2}\theta\right) + Q_3\sin\left(\frac{3}{2}\theta\right) \\ -\frac{1}{6}(Q_1+1)\cos\left(\frac{1}{2}\theta\right) + Q_4\cos\left(\frac{3}{2}\theta\right) \\ 0\end{pmatrix},
\end{aligned} \tag{29}$$

where

$$\begin{aligned}
Q_1 &= \frac{(2\lambda+6\mu)}{(\lambda+\mu)}, \quad Q_2 = \frac{(3\lambda-\mu)}{6(\lambda+\mu)}, \quad Q_3 = \frac{(45\lambda^2+138\lambda\mu+61\mu^2)}{90(\lambda+\mu)^2}, \\
Q_4 &= \frac{(-15\lambda^2+2\lambda\mu+49\mu^2)}{90(\lambda+\mu)^2}.
\end{aligned} \tag{30}$$

and in the case of homogeneous Dirichlet boundary conditions the displacements are of the form:

$$\tilde{\boldsymbol{u}}^{(\alpha_1)} = A_1(x_3)r^{\frac{1}{2}} \begin{pmatrix} -\sin\left(\frac{1}{2}\theta\right) + C_1 \sin\left(\frac{3}{2}\theta\right) \\ -C_1\cos\left(\frac{1}{2}\theta\right) + C_1\cos\left(\frac{3}{2}\theta\right) \\ 0 \end{pmatrix} + \partial_3^1 A_1(x_3) r^{\frac{3}{2}} \begin{pmatrix} 0 \\ 0 \\ C_2\sin\left(\frac{1}{2}\theta\right) \end{pmatrix}$$
$$+ \partial_3^2 A_1(x_3) r^{\frac{5}{2}} \begin{pmatrix} C_3\sin\left(\frac{1}{2}\theta\right) + C_4\sin\left(\frac{3}{2}\theta\right) \\ \frac{1}{6}C_1\cos\left(\frac{1}{2}\theta\right) - \frac{1}{6}C_1\cos\left(\frac{3}{2}\theta\right) \\ 0 \end{pmatrix} \tag{31}$$

where

$$C_1 = \frac{(3\lambda+7\mu)}{(\lambda+5\mu)}, \quad C_2 = \frac{2(\lambda+\mu)}{(\lambda+5\mu)}, \quad C_3 = \frac{(-3\lambda+\mu)}{6(\lambda+5\mu)}, \quad C_4 = -\frac{(3\lambda+7\mu)^2}{6(\lambda+5\mu)(7\lambda+11\mu)}. \tag{32}$$

The graphic representation of the primal eigen-function and the first two shadow-functions is presented in Figures 5, 6 for traction free and homogeneous Dirichlet boundary conditions, respectively, where $\lambda = 0.5769$ and $\mu = 0.3846$ (Young modulus $E = 1$ and Poisson ratio $\nu = 0.3$). The units of the material properties λ, μ and E are $\left[\frac{\mathrm{N}}{\mathrm{m}^2}\right]$. These values and units are chosen for simplicity of the presentation, although any other values, scales or units may be chosen.

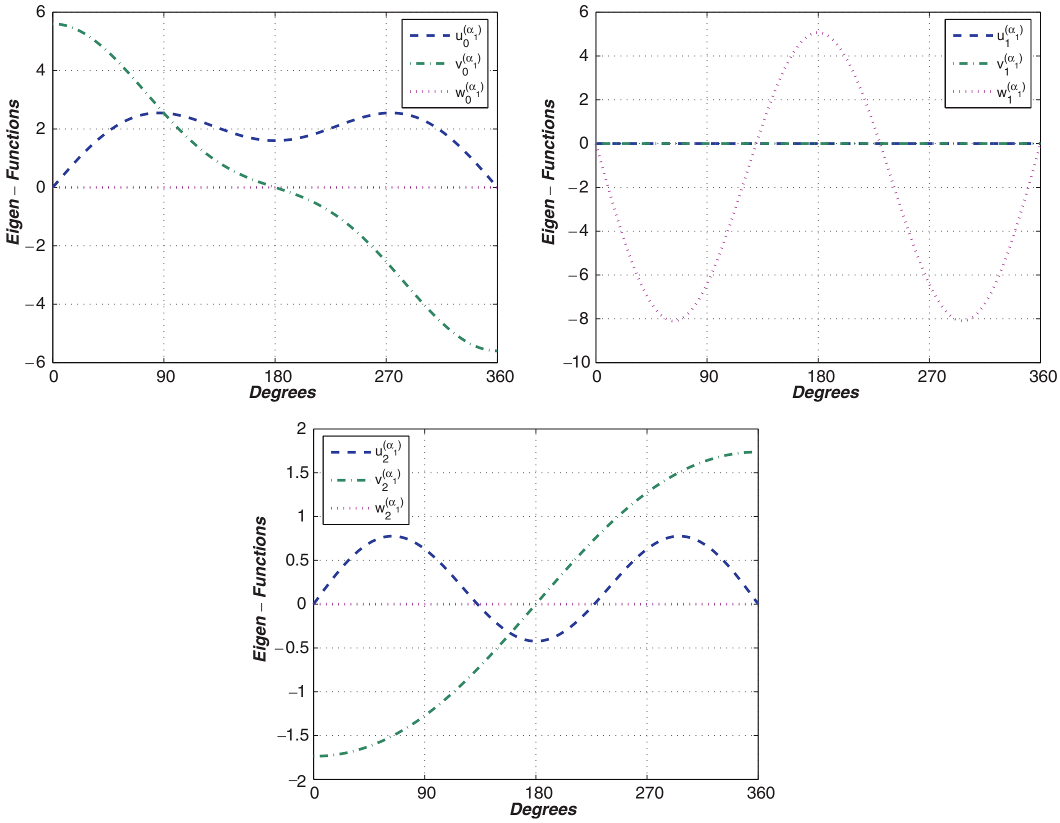

Figure 5. Primal and shadow-functions $\varphi_0^{(\alpha_1)}(\theta), \varphi_1^{(\alpha_1)}(\theta), \varphi_2^{(\alpha_1)}(\theta)$ for $\alpha_1 = \frac{1}{2}$, $\omega = 2\pi$, traction free boundary conditions, $\lambda = 0.5769$ and $\mu = 0.3846$.

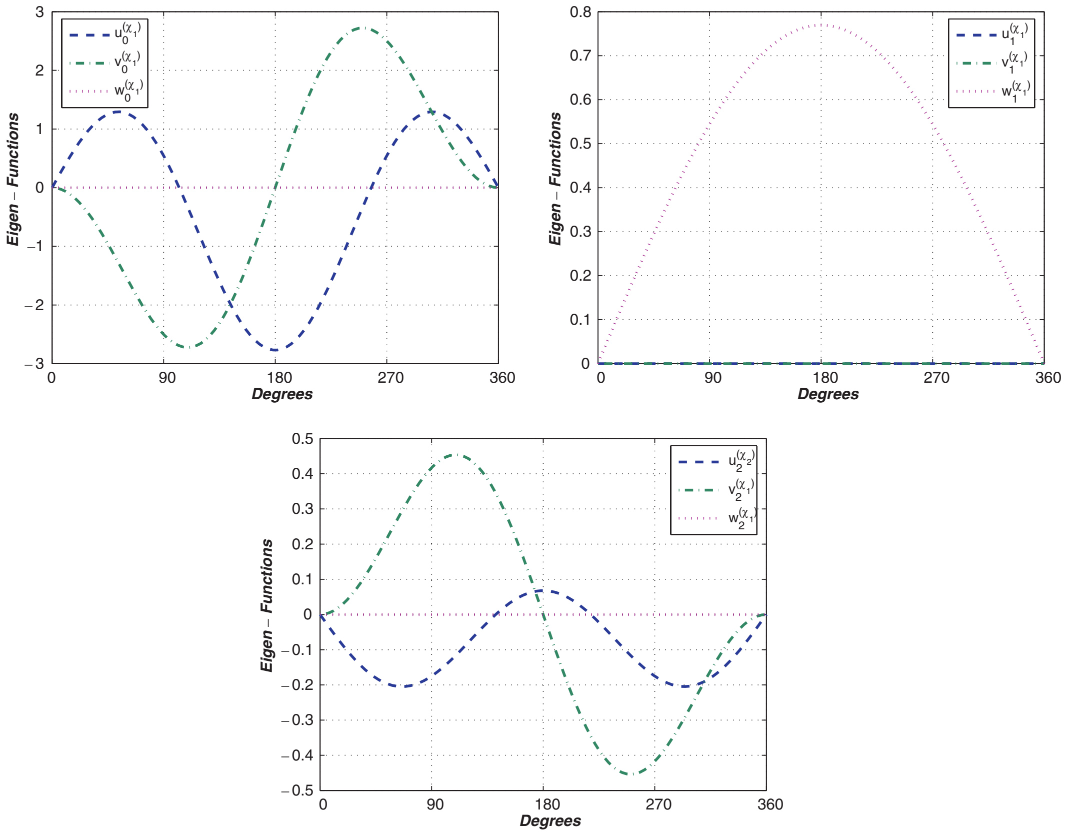

Figure 6. Primal and shadow-functions $\varphi_0^{(\alpha_1)}(\theta), \varphi_1^{(\alpha_1)}(\theta), \varphi_2^{(\alpha_1)}(\theta)$ for $\alpha_1 = \frac{1}{2}$, $\omega = 2\pi$, homogeneous Dirichlet boundary conditions, $\lambda = 0.5769$ and $\mu = 0.3846$.

Remark 3. Under the assumption of plane-strain and mode I loading, the classical 2-D solution $\boldsymbol{U}$ in the vicinity of a crack tip with traction free boundary conditions is:

$$\begin{Bmatrix} U_1 \\ U_2 \end{Bmatrix} = \frac{K_I(1+\nu)}{E\sqrt{2\pi}} r^{1/2} \begin{Bmatrix} \cos\left(\frac{1}{2}\tilde{\theta}\right)(\kappa - 1 + 2\sin^2\left(\frac{1}{2}\tilde{\theta}\right)) \\ \sin\left(\frac{1}{2}\tilde{\theta}\right)(\kappa + 1 - 2\cos^2\left(\frac{1}{2}\tilde{\theta}\right)) \end{Bmatrix} \tag{33}$$

where $\kappa = 3 - 4\nu$.

In this case A_1 in (28) is a constant so the relation between A_1 and the classical K_I for traction free boundary conditions is (see also (B.1) in Appendix B, for $\lambda = 0.5769$ and $\mu = 0.3846$):

$$\begin{aligned} &\frac{1.3K_I}{\sqrt{2\pi}} \cos\left(\tfrac{1}{2}\tilde{\theta}\right)\left(0.8 + 2\sin^2(\tilde{\theta})\right) = A_1\left(-2.6\sin\left(\tfrac{1}{2}(-\tilde{\theta}+\pi)\right) - \sin\left(\tfrac{3}{2}(-\tilde{\theta}+\pi)\right)\right) \\ &\frac{0.65K_I}{\sqrt{2\pi}}\left(2.6\cos\left(\tfrac{1}{2}\tilde{\theta}\right) - \cos\left(\tfrac{3}{2}\tilde{\theta}\right)\right) = A_1\left(2.6\cos\left(\tfrac{1}{2}\tilde{\theta}\right) - \cos\left(\tfrac{3}{2}\tilde{\theta}\right)\right) \\ &\frac{0.65K_I}{\sqrt{2\pi}} = A_1 \end{aligned} \tag{34}$$

which turns out to be independent of $\tilde{\theta}$.

Remark 4. The strain component ε_{33} computed using the displacements in (28), for the case where A_1 is constant, is:

$$\varepsilon_{33} = \frac{\partial^2 u_3}{\partial x_3^2} = 0. \tag{35}$$

On the other hand if plane-stress condition is assumed ε_{33} is give by (see (B.3)):

$$\varepsilon_{33} = \frac{\sigma_{11}}{E} - \frac{\nu}{E}(\sigma_{11} + \sigma_{22}) \quad \Rightarrow \quad \varepsilon_{33} = -\frac{\nu}{E}(\sigma_{11} + \sigma_{22}) = -0.923076 r^{-\frac{1}{2}} \sin(\tfrac{1}{2}\theta) \tag{36}$$

and therefore in 3-D the plane-stress assumption conditions can not hold in the vicinity of the singular point.

Remark 5. One may notice that the first term in (28) associated with $A_1(x_3)$ dominates as $r \to 0$, because the 'shadow functions' associated with derivatives of A_1 are multiplied by increasing orders of r. Therefore, $\lim_{r\to 0} J_{X_1}(s)$ regains the relationship given in (2).

3. Analytical and numerical computation of $J_{X_1}(s)$

Once the elastic solution in the vicinity of an edge was obtained, we are in the position to compute $J_{X_1}(s)$ both analytically and numerically using finite element methods. The purpose of computation is to show that numerical approximations of $J_{X_1}(s)$ are path independent for the problems considered. Although the area integral $J_{X_1}^{\text{area}}(s)$ contains larger errors in the numerical calculation due to the second numerical derivatives computed in the vicinity of the singular point, good approximation may be obtained when these derivatives are numerically computed with high order. We will show that in practical engineering problems, one may estimate $J_{X_1}(s)$ with good accuracy computing the path integral only (which is path-dependent in 3-D) at several radii of decreasing value, followed by Richardson's extrapolation.

We consider the six example problems with $\lambda = 0.5769$ and $\mu = 0.3846$ and either traction free or homogeneous Dirichlet boundary conditions on Γ_1 and Γ_2, see Table 1.

Because $\partial_3^n A_1^{(A)}(x_3) = \partial_3^n A_1^{(D)}(x_3) = 0$ for $n \geqslant 1$, the exact solution of examples (A) and (D) contains only the primal eigen-function, $\mathbf{\Phi}_0$, and the displacements represent a plane-strain situation. Examples (B) and (E) contain the shadow function

Table 1. Six example problems for which $J_{X_1}(X_3)$ is computed.

Example #	ESIF: $A(x_3)$	Boundary conditions over Γ_1, Γ_2
A	1	Traction free
B	$1 + x_3$	Traction free
C	$1 + x_3 + x_3^2$	Traction free
D	1	Homogeneous Dirichlet
E	$1 + x_3$	Homogeneous Dirichlet
F	$1 + x_3 + x_3^2$	Homogeneous Dirichlet

$\mathbf{\Phi}_1$ and the primal eigen-function $\mathbf{\Phi}_0$, whereas the two examples (C) and (F) contain two shadow functions $\mathbf{\Phi}_2$ and $\mathbf{\Phi}_1$ and the primal function $\mathbf{\Phi}_0$. The exact solutions of examples (A)–(F) are:

$$\tilde{\boldsymbol{u}}^{(A)}(r,\theta,x_3) = \begin{pmatrix} u_r^{(A)} \\ u_\theta^{(A)} \\ u_3^{(A)} \end{pmatrix} = r^{\frac{1}{2}} \begin{pmatrix} 2.6\sin\left(\frac{1}{2}\theta\right)+\sin\left(\frac{3}{2}\theta\right) \\ 4.6\cos\left(\frac{1}{2}\theta\right)+\cos\left(\frac{3}{2}\theta\right) \\ 0 \end{pmatrix} \tag{37}$$

$$\begin{aligned} \tilde{\boldsymbol{u}}^{(B)}(r,\theta,x_3) = \begin{pmatrix} u_r^{(B)} \\ u_\theta^{(B)} \\ u_3^{(B)} \end{pmatrix} &= (1+x_3) r^{\frac{1}{2}} \begin{pmatrix} 2.6\sin\left(\frac{1}{2}\theta\right)+\sin\left(\frac{3}{2}\theta\right) \\ 4.6\cos\left(\frac{1}{2}\theta\right)+\cos\left(\frac{3}{2}\theta\right) \\ 0 \end{pmatrix} \\ &+ r^{\frac{3}{2}} \begin{pmatrix} 0 \\ 0 \\ -2\sin\left(\frac{1}{2}\theta\right) - 3.066666\sin\left(\frac{3}{2}\theta\right) \end{pmatrix} \end{aligned} \tag{38}$$

$$\begin{aligned} \tilde{\boldsymbol{u}}^{(C)}(r,\theta,x_3) = \begin{pmatrix} u_r^{(C)} \\ u_\theta^{(C)} \\ u_3^{(C)} \end{pmatrix} &= (1+x_3+x_3^2) r^{\frac{1}{2}} \begin{pmatrix} 2.6\sin\left(\frac{1}{2}\theta\right)+\sin\left(\frac{3}{2}\theta\right) \\ 4.6\cos\left(\frac{1}{2}\theta\right)+\cos\left(\frac{3}{2}\theta\right) \\ 0 \end{pmatrix} \\ &+ (1+2x_3) r^{\frac{3}{2}} \begin{pmatrix} 0 \\ 0 \\ -2\sin\left(\frac{1}{2}\theta\right) - 3.066666\sin\left(\frac{3}{2}\theta\right) \end{pmatrix} \\ &+ 2r^{\frac{5}{2}} \begin{pmatrix} 0.23333\sin\left(\frac{1}{2}\theta\right) + 0.65644\sin\left(\frac{3}{2}\theta\right) \\ -0.76667\cos\left(\frac{1}{2}\theta\right) + 0.03244\cos\left(\frac{3}{2}\theta\right) \\ 0 \end{pmatrix} \end{aligned} \tag{39}$$

$$\tilde{\boldsymbol{u}}^{(D)}(r,\theta,x_3) = \begin{pmatrix} u_r^{(D)} \\ u_\theta^{(D)} \\ u_3^{(D)} \end{pmatrix} = r^{\frac{1}{2}} \begin{pmatrix} -\sin\left(\frac{1}{2}\theta\right) + 1.76923\sin\left(\frac{3}{2}\theta\right) \\ -1.76923\cos\left(\frac{1}{2}\theta\right) + 1.76923\cos\left(\frac{3}{2}\theta\right) \\ 0 \end{pmatrix} \tag{40}$$

$$\begin{aligned} \tilde{\boldsymbol{u}}^{(E)}(r,\theta,x_3) = \begin{pmatrix} u_r^{(E)} \\ u_\theta^{(E)} \\ u_3^{(E)} \end{pmatrix} &= (1+x_3) r^{\frac{1}{2}} \begin{pmatrix} -\sin(\frac{1}{2}\theta) + 1.76923\sin(\frac{3}{2}\theta) \\ -1.76923\cos(\frac{1}{2}\theta) + 1.76923\cos(\frac{3}{2}\theta) \\ 0 \end{pmatrix} \\ &+ r^{\frac{3}{2}} \begin{pmatrix} 0 \\ 0 \\ 0.76923\sin(\frac{1}{2}\theta) \end{pmatrix} \end{aligned} \tag{41}$$

$$\tilde{\boldsymbol{u}}^{(F)}(r,\theta,x_3)=\begin{pmatrix}u_r^{(F)}\\ u_\theta^{(F)}\\ u_3^{(F)}\end{pmatrix} = (1+x_3+x_3^2)r^{\frac{1}{2}}\begin{pmatrix}-\sin\left(\frac{1}{2}\theta\right)+1.76923\sin\left(\frac{3}{2}\theta\right)\\ -1.76923\cos\left(\frac{1}{2}\theta\right)+1.76923\cos\left(\frac{3}{2}\theta\right)\\ 0\end{pmatrix}$$
$$+(1+2x_3)r^{\frac{3}{2}}\begin{pmatrix}0\\ 0\\ 0.76923\sin(\frac{1}{2}\theta)\end{pmatrix}$$
$$+2r^{\frac{5}{2}}\begin{pmatrix}-0.08974\sin(\frac{1}{2}\theta)-0.15772\sin(\frac{3}{2}\theta)\\ 0.29487\cos(\frac{1}{2}\theta)-0.29487\cos(\frac{3}{2}\theta)\\ 0\end{pmatrix} \quad (42)$$

In the case of examples (A), (D) the ESIF is a constant and therefore the exact solutions $\tilde{\boldsymbol{u}}^{(A)}$, $\tilde{\boldsymbol{u}}^{(D)}$ are identical to the 2-D solution whereas example (B), (C), (E) and (F) represent a 3-D problem (containing either $\boldsymbol{\Phi}_0$ and $\boldsymbol{\Phi}_1$ or $\boldsymbol{\Phi}_0$, $\boldsymbol{\Phi}_1$ and $\boldsymbol{\Phi}_2$).

Consider now the domain Ω shown in Figure 4 defined by $r \in [0,1]$, $\theta \in [0,\omega]$, $x_3 \in [-1,1]\}$. If we prescribe the displacements boundary conditions to be one of the displacements shown in (37)–(42) (of examples $(A)-(F)$) on the surface $\partial\Omega - \Gamma_1 - \Gamma_2$, and let Γ_1 and Γ_2 be either free of tractions (in the case of examples (A)–(C)) or homogenous Dirichlet (in the case of examples (D)–(F)), then the displacements throughout all Ω are precisely as given in (37)-(42), respectively.

3.1. Computing $J_{X_1}(s)$ analytically

For each of the example problems (A)–(F) the exact solution is known, and therefore the path-area $J_{X_1}(s)$-integral may be computed analytically (the units of the $J_{X_1}(s)$ integral are: $[\frac{\mathrm{N}}{\mathrm{m}}]$). *Notice, however, that the* $\boldsymbol{X}$ *coordinate system must be used to represent all quantities for the computation of* $J_{X_1}(s)$. Thus, we provide in Appendix B the displacements (corresponding to (37)–(42)), strains and stresses in the $\boldsymbol{X}$ system for example problems (A)–(F).

We consider a circular path Γ of radius R, surrounding the crack front at point $s \equiv X_3$ along the crack on a plane perpendicular to the crack, as shown in Figure 7.

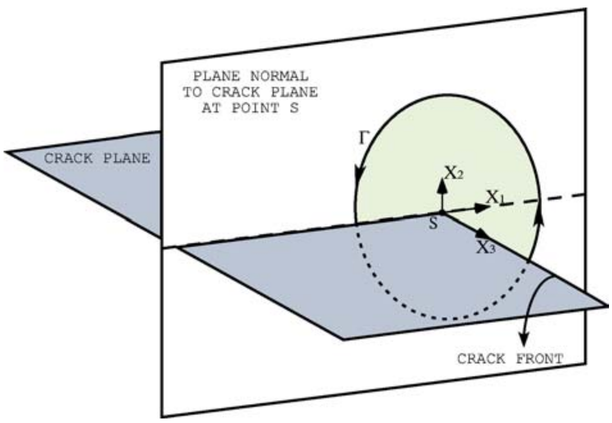

Figure 7. The path Γ and the area $A(\Gamma)$ enclosed by the path.

Because $J_{X_1}(X_3)$ contains a path integral and an area integral, we denote each by $J_{X_1}^{\text{path}}(X_3)$ and $J_{X_1}^{\text{area}}(X_3)$, respectively.

We show that $J_{X_1}(X_3)$ is path independent (the value of the integral is a function of X_3 only) for examples (A)–(F). The solutions of examples (A) and (D) are identical to a plane strain situation for which $J_{X_1}^{\text{area}}(X_3)$ vanishes and the path integral, $J_{X_1}^{\text{path}}(X_3)$ reduces to the well known J-integral in 2-D problems. The other four example problems $((B),(C),(E),(F))$ on the other hand, represent a general 3-D problem for which both the area and path integrals are R dependent. However, the $J_{X_1}(X_3)$-integral $(J_{X_1}(X_3) = J_{X_1}^{\text{path}}(X_3) - J_{X_1}^{\text{area}}(X_3))$ is path independent as shown in the sequel.

The displacements, strains and stresses for example problems (A)–(F) (provided in Appendix B) are used to compute $J_{X_1}(s)$ analytically:

3.1.1. *Example A*

The area-integral $J_{X_1}^{\text{area}(A)}(X_3) \equiv 0$, so

$$J_{X_1}^{(A)}(X_3) = J_{X_1}^{\text{path}(A)}(X_3) = 13.533. \tag{43}$$

As expected $J_{X_1}^{(A)}(X_3)$ is a constant and therefore path independent.

3.1.2. *Example B*

The path-integral for example problem (B) is:

$$J_{X_1}^{\text{path}(B)}(X_3) = \int_{-\pi}^{\pi} \left(Wn_1 - T_\beta \cdot \partial_1 U_\beta\right)_R R\,\mathrm{d}\tilde{\theta} = 13.533(1+X_3)^2 + 8.69978R^2, \tag{44}$$

and the area-integral is:

$$J_{X_1}^{\text{area}(B)}(X_3) = \int_0^R \int_{-\pi}^{\pi} \partial_3\left(\sigma_{\beta 3}\partial_1 U_\beta\right) r\,\mathrm{d}r\,\mathrm{d}\tilde{\theta} = 8.69978R^2. \tag{45}$$

Therefore $J_{X_1}^{(B)}(X_3)$ is:

$$J_{X_1}^{(B)}(X_3) = J_{X_1}^{\text{path}(B)}(X_3) - J_{X_1}^{\text{area}(B)}(X_3) = 13.533(1+X_3)^2. \tag{46}$$

Notice that $J_{X_1}(X_3)$ for example problem (B) is path-independent, however both the path and area integrals are path-dependent having a $\mathcal{O}(R^2)$ dependency (the radius of the circular path).

At the point $X_3 = -0.2$ along the crack front:

$$J_{X_1}^{(B)}(X_3 = -0.2) = 19.48752. \tag{47}$$

On the other hand, we may use (35) to compute the stress intensity factor at $X_3 = -0.2$:

$$K_I = 3.85635A_1(X_3) = 3.85635(1-(-0.2)). \tag{48}$$

Now assuming that (2) can be extended beyond the situation of plane-strain (to our best knowledge, a proof that $J_{X_1} = \mathcal{G}$ does not exist for 3-D domains) and taking E^* for plane strain $E^*(E=1, \nu=0.3) = 1.0989$:

$$\mathcal{G}(X_3 = -0.2) = \frac{K_I^2}{E^*} = \frac{(3.85635(1-(-0.2)))^2}{1.0989} = 19.48752, \tag{49}$$

we obtain the same value as in (47).

3.1.3. *Example C*

The path-integral for example problem (C) is:

$$\begin{aligned} J_{X_1}^{\text{path}(C)}(X_3) &= \int_{-\pi}^{\pi} \left(Wn_1 - T_\beta \cdot \partial_1 U_\beta\right)_R \; R \, \mathrm{d}\tilde{\theta} \\ &= 13.533(1 - X_3 + X_3^2)^2 + 52.19871(0.5 - X_3 + X_3^2)R^2 - 21.78168R^4, \end{aligned} \tag{50}$$

and the area integral is:

$$\begin{aligned} J_{X_1}^{\text{area}(C)}(X_3) &= \int_0^R \int_{-\pi}^{\pi} \partial_3 \left(\sigma_{\beta 3}\partial_1 U_\beta\right) r \, \mathrm{d}r \, \mathrm{d}\tilde{\theta} \\ &= 52.19871(0.5 - X_3 + X_3^2)R^2 - 21.78168R^4. \end{aligned} \tag{51}$$

Therefore $J_{X_1}^{(C)}(X_3)$ is:

$$J_{X_1}^{(C)}(X_3) = J_{X_1}^{\text{path}(C)}(X_3) - J_{X_1}^{\text{area}(C)}(X_3) = 13.533(1 - X_3 + X_3^2)^2. \tag{52}$$

The value of $J_{X_1}(X_3)$ for example problem (C) is path-independent, but both the path and area integrals are path-dependent having a $\mathcal{O}(R^2) + \mathcal{O}(R^4)$ dependency.

Again, let us compute the value of $J_{X_1}^{(C)}$ at $X_3 = -0.2$, (52) results in:

$$J_{X_1}^{(C)}(X_3 = -0.2) = 20.80834. \tag{53}$$

From (35) one obtains:

$$K_I = 3.85635 A_1(X_3) = 3.85635(1 - (-0.2) + (-0.2)^2) \tag{54}$$

and $\mathcal{G}$ for plane strain situation is:

$$\mathcal{G}(X_3 = -0.2) = \frac{K_I^2}{E^*} = \frac{(3.85635(1-(-0.2)+(-0.2)^2))^2}{1.0989} = 20.80834. \tag{55}$$

As in example problem (B), we obtain the same value of $\mathcal{G}(X_3 = -0.2)$ as in (53).

3.1.4. *Example D*

The area-integral $J_{X_1}^{\text{area}(D)}(X_3) \equiv 0$, so

$$J_{X_1}^{(D)}(X_3) = J_{X_1}^{\text{path}(D)}(X_3) = -3.60571, \tag{56}$$

and because example (D) represents a plane strain situation, $J_{X_1}^{(D)}(X_3)$ is path independent.

3.1.5. *Example E*
The path-integral $J_{X_1}(X_3)$ of example problem (E) is:

$$J_{X_1}^{\mathrm{path}(E)}(X_3) \;=\; \int_{-\pi}^{\pi} \left(Wn_1 - T_\beta \cdot \partial_1 U_\beta\right)_R R\,\mathrm{d}\tilde{\theta} = -3.60346(1-X_3)^2 + 1.42280R^2, \tag{57}$$

and the area-integral is:

$$J_{X_1}^{\mathrm{area}(E)}(X_3) = \int_0^R \int_{-\pi}^{\pi} \partial_3\left(\sigma_{\beta 3}\partial_1 U_\beta\right) r\,\mathrm{d}r\,\mathrm{d}\tilde{\theta} = 1.42280R^2. \tag{58}$$

Therefore $J_{X_1}^{(E)}(X_3)$ is:

$$J_{X_1}^{(E)}(X_3) = J_{X_1}^{\mathrm{path}(E)}(X_3) - J_{X_1}^{\mathrm{area}(E)}(X_3) = -3.60346(1-X_3)^2 \tag{59}$$

$J_{X_1}(X_3)$ for example problem (E) is path-independent, and as seen previously both the path and area integrals are path-dependent having a $\mathcal{O}(R^2)$ dependency.

3.1.6. *Example F*
The path-integral of $J_{X_1}(X_3)$ for example problem (F) is:

$$\begin{aligned} J_{X_1}^{\mathrm{path}(F)}(X_3) \;&=\; \int_{-\pi}^{\pi} \left(Wn_1 - T_\beta \cdot \partial_1 U_\beta\right)_R R\mathrm{d}\tilde{\theta} \\ &=\; -3.60346(1+X_3+X_3^2)^2 + 8.53677(0.5+X_3+X_3^2)R^2 + 1.21678R^4 \end{aligned} \tag{60}$$

and the area-integral is:

$$\begin{aligned} J_{X_1}^{\mathrm{area}(F)}(X_3) \;&=\; \int_0^R \int_{-\pi}^{\pi} \partial_3\left(\sigma_{\beta 3}\partial_1 U_\beta\right) r\,\mathrm{d}r\,\mathrm{d}\tilde{\theta} \\ &=\; 8.53677(0.5+X_3+X_3^2)R^2 + 1.21678R^4. \end{aligned} \tag{61}$$

Therefore $J_{X_1}^{(F)}(X_3)$ is:

$$J_{X_1}^{(F)}(X_3) = J_{X_1}^{\mathrm{path}(F)}(X_3) - J_{X_1}^{\mathrm{area}(F)}(X_3) = -3.60346(1+X_3+X_3^2)^2. \tag{62}$$

The value of $J_{X_1}(X_3)$ for example problem (F) is path-independent, but both the path and area integrals are path-dependent having a $\mathcal{O}(R^2) + \mathcal{O}(R^4)$ dependency.

3.2. Numerical computation of $J_{X_1}(s)$ for examples (A)–(F)

As the $J_{X_1}(s)$-integral is frequently used in numerical methods, we herein compute its value for examples (A)–(F) by p-finite element methods (Szabb and Babuŝka, 1991), using the commercial finite element code StressCheck. The specific code has been chosen because of the p-FE technology, and the possibility to post-process the results using a COM interface based on VisualBasic. The domain Ω is discretized by using a mesh with geometrical progression towards the singular edge with a factor of 0.17, having six layers of elements. In X_3 direction, a uniform discretization using five elements has been adopted. There are 240 3-D elements (hexahedral and pentahedral), over which the polynomial degree, using trunk space has been increased from 1 to 7 (at $p=7$ the FE model contains 31,614 degrees of freedom) to ensure the convergence of the results. The estimated error in energy norm at $p=7$ is 0.25%. The finite element mesh is shown in Figure 8.

We specify over the entire boundaries of the domain Dirichlet boundary conditions according to the selected examples (A)–(F), (37)–(42). This implies that the solution at any point r, θ, x_3 is exactly (37)–(42).

For the numerical computation of $J_{X_1}(X_3)$ in (3), the finite element approximations of $U_i(r, \tilde{\theta}, X_3)$, $\varepsilon_{ij}(r, \tilde{\theta}, X_3)$, and $\sigma_{ij}(r, \tilde{\theta}, X_3)$ are used, and the integral is computed numerically using Gaussian quadrature of order 10 for each integration variable. The use of a quadrature order of 32 does not change the results considerably. The numerical computation of $J_{X_1}(X_3)$ involves both path and area integrals, where the integration area includes the singular point. Because of the poor accuracy of the numerical solution (stresses, strains and displacements) in the vicinity of the singular point, we expect the numerical calculation of the area integral to be of a lower accuracy compared to the path integral. Moreover, the components of the area integral include numerical second derivatives of the displacements, which adds to the inaccuracies of the numerical results. The second derivative was computed using a second order difference approximation for partial derivative, i.e.:

$$\begin{aligned}\frac{\partial^2 U_2(X_1,X_2,X_3)}{\partial X_1 \partial X_3} = \frac{1}{2\triangle X_1}\Bigg(&\frac{U_2(X_1+\triangle X_1,X_2,X_3+\triangle X_3)-U_2(X_1+\triangle X_1,X_2,X_3-\triangle X_3)}{2\triangle X_3}\\ &-\frac{U_2(X_1-\triangle X_1,X_2,X_3+\triangle X_3)-U_2(X_1-\triangle X_1,X_2,X_3-\triangle X_3)}{2\triangle X_3}\Bigg)+\mathcal{O}(\triangle X_1^2, \triangle X_3^2).\end{aligned} \tag{63}$$

The numerical results of $J_{X_1}^{\text{path}}$, $J_{X_1}^{\text{area}}$ and J_{X_1} of each of the examples extracted from the FE solution at $p=7$ for different R-values are summarized in Appendix C in Tables C1–C6. We chose a random point $X_3=-0.2$ along the crack front at which the computations are performed. The results demonstrate that the area integral is computed with small numerical errors due to the refined FE model and the second-order numerical derivatives and its contribution to the total J_{X_1} is progressively smaller as $R \to 0$. The numerical value of J_{X_1} is less than 0.4% error compared to the exact value, for all inspected R's.

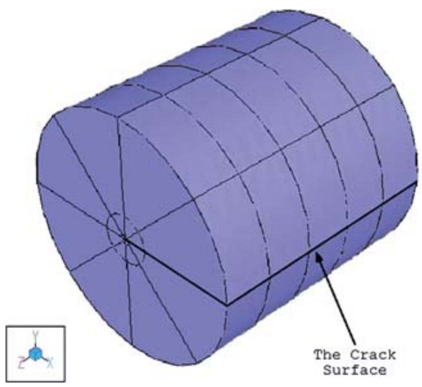

Figure 8. The p-FE mesh.

The relative error in percentage, defined as:

$$100\frac{J_{X_1}^{\text{Num}} - J_{X_1}^{\text{Exact}}}{J_{X_1}^{\text{Exact}}}$$

is plotted as a function of R in Figure 9, demonstrating that indeed the numerical approximation of J_{X_1} is closely path independent, where the deviations are attributed to the numerical errors of the FE solution.

To avoid the computation of the area integral, which requires high numerical derivatives as well as data in the close vicinity of the singular point, often the path integral alone is computed in a plane perpendicular to the crack front, i.e. the $J_{X_1}^{\text{path}}$. The $J_{X_1}^{\text{path}}$-integral has an $\mathcal{O}(R^2)$ dependency, which is demonstrated by plotting in Figure 10 the relative error of the numeric calculation of $J_{X_1}^{\text{path}}$ ($100 \cdot \frac{(J_{X_1} - J_{X_1}^{\text{path}})}{J_{X_1}}$), at different values of R's for example problems $(B)-(C)$, and $(E)-(F)$.

Using Richardson's extrapolation with the remainder behaving as $\mathcal{O}(R^2)$ for numeric $J_{X_1}^{\text{path}}$ at decreasing radii, one may obtains $J_{X_1}^{\text{path}}|_{R\to 0} = J_{X_1}$. In Tables 2–5 we demonstrate the good results obtained by Richardson's extrapolation for example problems $(B)-(C)$ and $(E)-(F)$.

3.3. The compact tension specimen - an example problem of engineering importance

As an example of engineering relevance, we consider the computation of J_{X_1} at two arbitrary points along the crack front of a compact tension specimen (CTS).

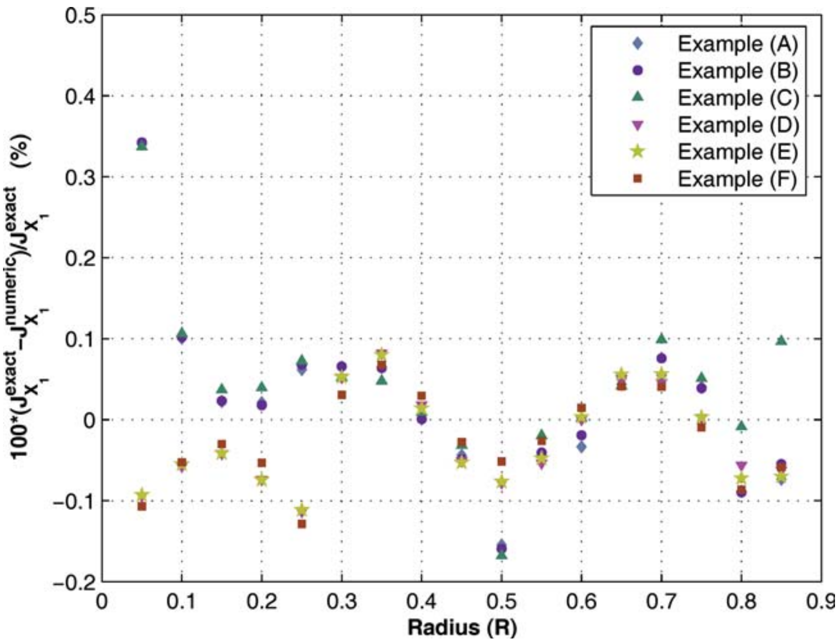

Figure 9. Relative error of J_{X_1} computed numerically at different paths for example problems (A)–(F).

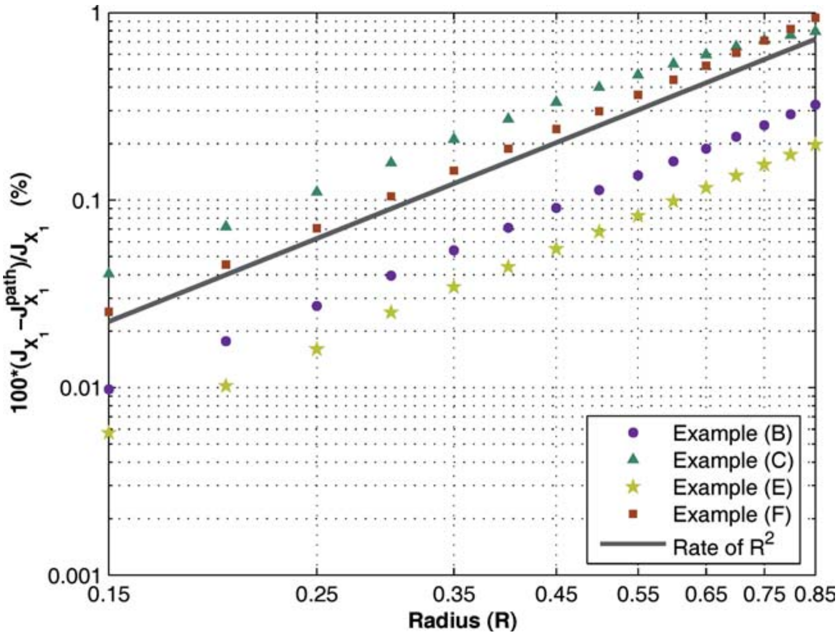

Figure 10. Relative error of $J_{X_1}^{\text{path}}$ for example problems (B)–(C), and (E)–(F).

Consider the classical CTS as shown in Figure 11. We select the length units in the figure to be [cm], however any other units may be chosen. For simplicity the units of material properties λ, μ and E are $[\frac{\text{N}}{\text{cm}^2}]$, ($\lambda = 0.5769$, $\mu = 0.3846$, $E = 1$, $\nu = 0.3$), and therefore the units of J_{X_3} integral and K_I are $[\frac{\text{N}}{\text{cm}}]$ and $\frac{\text{N}}{\text{cm}^2}\sqrt{\text{cm}}$, respectively. The CTS is subject to bearing loads at the tearing holes having an equivalent force in the X_2 direction and constant in X_3 direction, as presented in Figure 12. All other faces are traction free. The thickness of the specimen is 2 ranging from $-1 < X_3 < 1$. The specimen is subjected to a tension load of 100 [N] such that only Mode I is excited along the crack front. Although the boundary conditions and geometry is independent of X_3, due to the vertex singularities and the free faces at $X_3 = \pm 1$ the solution is X_3 dependent and approximating it by a 2-D plane strain solution results in modeling-errors.

The CTS is discretized by using a p-FEM mesh, with geometrical progression towards the singular edge with a factor of 0.15 where the smallest layer in the vicinity of the edge is at $r = 0.15$. In X_3 direction we also use a mesh graded in a geometrical progression close to the vertex singularity at $X_3 = \pm 1$. Smallest layer in the vicinity of the vertex is $-1 < X_3 < -1 + 0.15^2$, $1 < X_3 < 1 - 0.15^2$. A finite element analysis was performed, increasing the polynomial order of the elements from $p = 1$ to $p = 7$. At $p = 7$ the estimated relative error in energy norm is 2.52%.

The values of J_{X_1}, $J_{X_1}^{\text{path}}$ and $J_{X_1}^{\text{area}}$ using FE solution at $p = 7$ for different R-values at two selected points $X_3 = -0.2$ and $X_3 = -0.4$ are summarized in Table 6. The smallest radius was chosen to be $R = 0.2$ because the smallest elements in the vicinity of the singular edge are of radius of 0.15 and the numerical solution in these elements are of low accuracy. The maximum value of J_{X_1} at $X_3 = -0.2$ is $J_{X_1}(X_3 = -0.2)|_{R=0.2} = 34397.25567$ whereas the minimum value is $J_{X_1}(X_3 = -0.2)|_{R=0.3} = 34178.97096$. The relative error between these two values is:

Table 2. Example problem (B): Richardson extrapolation. $J_{X_1}^{(B)}(-0.2) = 19.48752$.

R	$J_{X_1}^{\text{path}}(-0.2)$				
$R = 0.80$	25.07020				
		19.37594			
$R = 0.70$	23.73561		19.76433		
		19.54521		19.51013	
$R = 0.60$	22.62387		19.61094		19.02800
		19.57725		19.15469		19.75347
$R = 0.50$	21.69296		19.30749		19.63630
		19.42837		19.53959	
$R = 0.40$	20.87771		19.47874		
		19.46031			
$R = 0.30$	20.25760				

Table 3. Example problem (C): Richardson extrapolation. $J_{X_1}^{(C)}(-0.2) = 20.80834$.

R	$J_{X_1}^{\text{path}}(-0.2)$					
$R = 0.80$	36.58996					
		27.64889				
$R = 0.70$	34.49440		20.82879			
		24.67647		20.95895		
$R = 0.60$	31.88964		20.90734		20.43340	
		22.83948		20.57150		20.93766
$R = 0.50$	29.12431		20.68397		20.85622	
		21.64991		20.79904		
$R = 0.40$	26.43353		20.76888			
		21.09129				
$R = 0.30$	24.09630					

Table 4. Example problem (E): Richardson extrapolation. $J_{X_1}^{(E)}(-0.2) = -5.18898$.

R	$J_{X_1}^{\text{path}}(-0.2)$					
$R = 0.80$	−4.28200					
		−5.16507				
$R = 0.70$	−4.48897		−5.23855			
		−5.19709		−5.18768		
$R = 0.60$	−4.67684		−5.20785		−5.11896	
		−5.20234		−5.13702		−5.22808
$R = 0.50$	−4.83741		−5.16074		−5.21046	
		−5.17938		−5.19571		
$R = 0.40$	−4.96052		−5.18654			
		−5.18392				
$R = 0.30$	−5.05826					

Table 5. Example problem (F): Richardson extrapolation. $J_{X_1}^{(F)}(-0.2) = -5.540680$.

R	$J_{X_1}^{\mathrm{path}}(-0.2)$					
$R = 0.80$	−1.00392					
		−5.89582				
$R = 0.70$	−2.15046		−5.59045			
		−5.76273		−5.53685		
$R = 0.60$	−3.10882		−5.55811		−5.47049	
		−5.66300		−5.48793		−5.58633
$R = 0.50$	−3.88926		−5.51143		−5.56762	
		−5.57935		−5.55162		
$R = 0.40$	−4.49770		−5.54108			
		−5.55509				
$R = 0.30$	−4.96031					

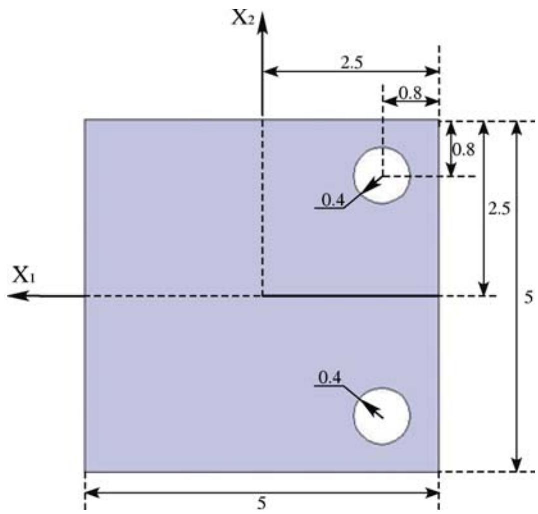

Figure 11. Dimensions of CTS. The thickness of the specimen is 2 ranging from $-1 < X_3 < 1$.

$$\frac{100(J_{X_1}|_{\max} - J_{X_1}|_{\min})}{J_{X_1}|_{\max}} = \frac{100(34397.25567 - 34178.97096)}{34397.25567} = 0.63460\% \tag{64}$$

thus the relative error is less than 1% (recall that estimated relative error in energy norm in the FE analysis is 2.52%).

The maximum/minimum values of J_{X_1} at $X_3 = -0.4$ are $J_{X_1}(X_3 = -0.4)|_{R=0.2} =$ 33812.02876 and 33602.06610. The relative error between these two values is:

$$\frac{100(J_{X_1}|_{\max} - J_{X_1}|_{\min})}{J_{X_1}|_{\max}} = \frac{100(33812.02876 - 33602.06610)}{33812.02876} = 0.62097\% \tag{65}$$

again the relative error is less than 1%.

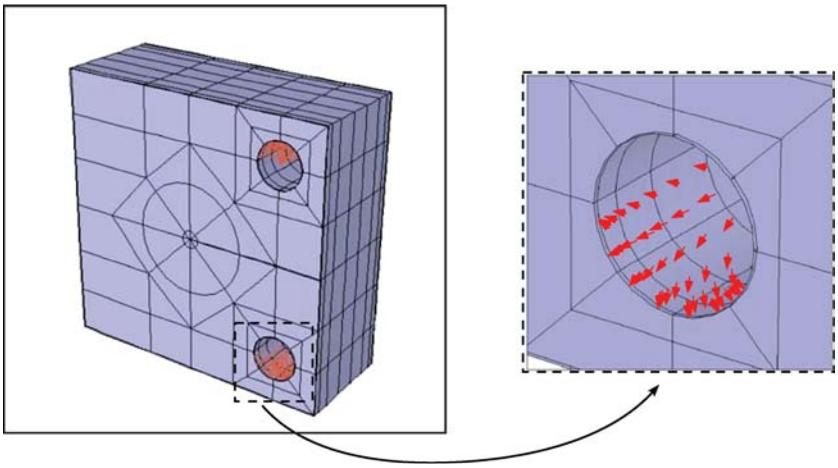

Figure 12. p-FEM model of the CTS with a bearing load (the loading at the upper hole is as in the shown lower hole, in the opposite direction).

Table 6. Numerical values of J_{X_1}, $J_{X_1}^{\text{path}}$ and $J_{X_1}^{\text{area}}$ at $X_3=-0.2$ and $X_3=-0.4$ for the CTS.

	Numerical results, $X_3=-0.2$			Numerical results, $X_3=-0.4$		
	J_{X_1}	$J_{X_1}^{\text{path}}$	$J_{X_1}^{\text{area}}$	J_{X_1}	$J_{X_1}^{\text{path}}$	$J_{X_1}^{\text{area}}$
$R=0.85$	34346.76585	32387.57008	−1959.19578	33772.13377	32073.86886	−1698.26491
$R=0.80$	34323.39161	32480.46959	−1842.92202	33749.77839	32122.41412	−1627.36426
$R=0.75$	34287.64206	32565.91838	−1721.72368	33713.12905	32163.75753	−1549.37152
$R=0.70$	34258.20391	32667.72166	−1590.48225	33680.92656	32222.75233	−1458.17423
$R=0.65$	34242.12139	32788.89236	−1453.22903	33660.88911	32303.26426	−1357.62485
$R=0.60$	34243.44680	32931.95563	−1311.49117	33658.67247	32409.11732	−1249.55515
$R=0.55$	34279.14826	33108.72044	−1170.42783	33690.51300	32552.99582	−1137.51718
$R=0.50$	34286.36396	33265.86787	−1020.49609	33706.66013	32683.32129	−1023.33884
$R=0.45$	34304.05709	33412.78316	−891.27393	33724.30692	32808.74824	−915.55868
$R=0.40$	34276.35140	33511.31953	−765.03187	33696.70770	32891.96010	−804.74760
$R=0.35$	34233.05917	33596.36112	−636.69803	33658.24510	32966.53911	−691.70599
$R=0.30$	34178.97096	33677.65453	−501.31644	33602.06610	33041.70858	−560.35752
$R=0.25$	34281.17603	33896.62084	−384.55519	33700.45273	33256.69113	−443.76161
$R=0.20$	34397.25567	34120.94327	−276.41240	33812.02876	33482.75676	−329.27201

4. Summary and conclusion

The extension of the Cherepanov–Rice J integral to three dimensional domains, resulting in a path-area integral evaluated at a point s along the crack front $J_{X_1}(s)$, has been extensively used to compute edge stress intensity functions at any point s. Past derivations assume either a plane stress/strain situation, or a restriction on the integration path such that $R \to 0$ to ensure it's path independency.

Herein we have shown that for more general three-dimensional states of stress under mode I loading, $J_{X_1}(s)$ is a *path-area-independent* integral, hence, its use is advocated. We have used the exact 3-D asymptotic solution in the vicinity of a crack front in a three-dimensional elastic domain derived explicitly following the general framework in Costabel et al. (2004) in order to check path independency.

Although one may estimate pointwise edge stress intensity functions at point s along the crack front by equating the $J_{X_1}(s)$ -integral to the pointwise energy release rate (under the assumption of plane strain), this connection for 3-D domains has not been yet validated by a proof (to our best knowledge). Nevertheless, numerical evidence suggests that this relationship may be provable.

Using the finite element method in conjunction with Richardson's extrapolation one may compute the path integral $J_{X_1}(s)^{\text{path}}$ alone at decreasing values of R and extrapolate to the limit $R \to 0$. In this case the *path-dependent* $J_{X_1}(s)^{\text{path}}$ integral converges to $J_{X_1}(s)$ as $R \to 0$.

Acknowledgement

The authors gratefully acknowledge an anonymous referee for valuable and constructive comments, leading to improvements in the presentation and context.

Notes

[1] Stresscheck is trademark of Engineering Software Research and Development, Inc, St.Louis, MO, USA

Appendix A: The 2-D J-integral path independency

In order to show the path independency of J, let us choose a close path such as $\Gamma^* = \Gamma_1 + \Gamma_2 + \Gamma_3 + \Gamma_4$, enclosing an area $A(\Gamma^*)$, see Figure 13. By using Green's theorem equation (1) becomes:

$$\int_{\Gamma^*} (W \mathrm{d}X_2 - \boldsymbol{T} \cdot \partial_1 \boldsymbol{U} \mathrm{d}s) = \int_{A(\Gamma^*)} \left(\partial_1 W - \partial_\gamma \left(\sigma_{\beta\gamma} \partial_1 U_\beta\right)\right) \mathrm{d}X_1 \mathrm{d}X_2. \tag{A.1}$$

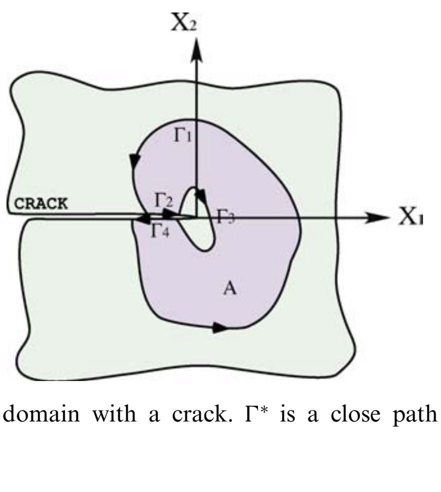

Figure 13. Two dimensional domain with a crack. Γ^* is a close path enclosing an area $A(\Gamma^*)$.

Using the chain rule, the strain energy density (first term of the area integral in (A.1)) is:

$$\partial_1 W = \frac{\partial W}{\partial \varepsilon_{\beta\gamma}} \cdot \frac{\partial \varepsilon_{\beta\gamma}}{\partial X_1} = \sigma_{\beta\gamma} \partial_1 \varepsilon_{\beta\gamma}. \tag{A.2}$$

Substituting relation (A.2) into (A.1) and using the symmetric relation of the stress tensor ($\sigma_{\beta\gamma} = \sigma_{\gamma\beta}$), the area integral is reduced to:

$$\int_{\Gamma^*} (W \mathrm{d}X_2 - \boldsymbol{T} \cdot \partial_1 \boldsymbol{U} \mathrm{d}s) = \int_{A(\Gamma^*)} \left(\sigma_{\beta\gamma} \partial_\gamma \left(\partial_1 U_\beta\right) - \partial_\gamma \left(\sigma_{\beta\gamma} \partial_1 U_\beta\right)\right) \mathrm{d}X_1 \mathrm{d}X_2 \tag{A.3}$$

because of the equilibrium equation without body forces, $\partial_\gamma \sigma_{\beta\gamma} = 0$, the area integral vanishes, so:

$$\int_{\Gamma^*} (W \mathrm{d}X_2 - \boldsymbol{T} \cdot \partial_1 \boldsymbol{U} \mathrm{d}s) = 0. \tag{A.4}$$

The path integrals over Γ_2 and Γ_4 vanish because $\mathrm{d}X_2 = 0$ and either $\boldsymbol{T} = 0$ or $\boldsymbol{U} = 0$ so that $\partial_1 \boldsymbol{U} = 0$ on both paths. By changing the direction of integration on Γ_3 , equation (A.4) is simplified:

$$\int_{\Gamma_1} (W \mathrm{d}X_2 - \boldsymbol{T} \cdot \partial_1 \boldsymbol{U} \mathrm{d}s) = \int_{\Gamma_3} (W \mathrm{d}X_2 - \boldsymbol{T} \cdot \partial_1 \boldsymbol{U} \mathrm{d}s) \equiv J. \tag{A.5}$$

The paths Γ_1 and Γ_3 are randomly selected, so the right hand side as well as the left hand side of relation (A.5) may be considered as an invariant where Γ is a path in the domain which starts at one edge and ends at the other edge of the crack.

Appendix B: Displacements, strains and stresses in Cartesian coordinates for example problems $(A)-(F)$

The expressions for the computation of the $J_{X_1}(s)$-integral are given in Polar coordinate system $(r, \tilde{\theta}, X_3)$. Therefore, we provide herein the displacements, strains and stresses in the required system.

B. 1. Displacements, strains and stresses for example problem (A)

$$\begin{aligned}
U_1^{(A)}\left(r, \tilde{\theta}, X_3\right) &= r^{\frac{1}{2}} \left(2.6 \cos\left(\frac{1}{2}\tilde{\theta}\right) - \cos\left(\frac{3}{2}\tilde{\theta}\right)\right) \\
U_2^{(A)}\left(r, \tilde{\theta}, X_3\right) &= r^{\frac{1}{2}} \left(4.6 \sin\left(\frac{1}{2}\tilde{\theta}\right) - \sin\left(\frac{3}{2}\tilde{\theta}\right)\right) \\
U_3^{(A)}\left(r, \tilde{\theta}, X_3\right) &= 0
\end{aligned} \tag{B.1}$$

$$
\begin{aligned}
\varepsilon_{11}^{(A)}\left(r,\tilde{\theta},X_3\right) &= r^{-\frac{1}{2}}\left(0.3\cos\left(\frac{1}{2}\tilde{\theta}\right)+0.5\cos\left(\frac{5}{2}\tilde{\theta}\right)\right)\\
\varepsilon_{22}^{(A)}\left(r,\tilde{\theta},X_3\right) &= r^{-\frac{1}{2}}\left(1.3\cos\left(\frac{1}{2}\tilde{\theta}\right)-0.5\cos\left(\frac{5}{2}\tilde{\theta}\right)\right)\\
\varepsilon_{33}^{(A)}\left(r,\tilde{\theta},X_3\right) &= 0\\
\varepsilon_{12}^{(A)}\left(r,\tilde{\theta},X_3\right) &= r^{-\frac{1}{2}}\left(-0.5\sin\left(\frac{1}{2}\tilde{\theta}\right)+0.5\sin\left(\frac{5}{2}\tilde{\theta}\right)\right)\\
\varepsilon_{13}^{(A)}\left(r,\tilde{\theta},X_3\right) &= 0\\
\varepsilon_{23}^{(A)}\left(r,\tilde{\theta},X_3\right) &= 0
\end{aligned}
\tag{B.2}
$$

and

$$
\begin{aligned}
\sigma_{11}^{(A)}\left(r,\tilde{\theta},X_3\right) &= r^{-\frac{1}{2}}\left(1.153845\cos\left(\frac{1}{2}\tilde{\theta}\right)+0.384615\cos\left(\frac{5}{2}\tilde{\theta}\right)\right)\\
\sigma_{22}^{(A)}\left(r,\tilde{\theta},X_3\right) &= r^{-\frac{1}{2}}\left(1.923075\cos\left(\frac{1}{2}\tilde{\theta}\right)-0.384615\cos\left(\frac{5}{2}\tilde{\theta}\right)\right)\\
\sigma_{33}^{(A)}\left(r,\tilde{\theta},X_3\right) &= r^{-\frac{1}{2}}0.923076\cos\left(\frac{1}{2}\tilde{\theta}\right)\\
\sigma_{12}^{(A)}\left(r,\tilde{\theta},X_3\right) &= r^{-\frac{1}{2}}\left(-0.384615\sin\left(\frac{1}{2}\tilde{\theta}\right)+0.384615\sin\left(\frac{5}{2}\tilde{\theta}\right)\right)\\
\sigma_{13}^{(A)}\left(r,\tilde{\theta},X_3\right) &= 0\\
\sigma_{23}^{(A)}\left(r,\tilde{\theta},X_3\right) &= 0
\end{aligned}
\tag{B.3}
$$

B. 2 . Displacements, strains and stresses for example problem (B)

$$
\begin{aligned}
U_{1}^{(B)}\left(r,\tilde{\theta},X_3\right) &= r^{\frac{1}{2}}\left(1-X_3\right)\left(2.6\cos\left(\frac{1}{2}\tilde{\theta}\right)-\cos\left(\frac{3}{2}\tilde{\theta}\right)\right)\\
U_{2}^{(B)}\left(r,\tilde{\theta},X_3\right) &= r^{\frac{1}{2}}\left(1-X_3\right)\left(4.6\sin\left(\frac{1}{2}\tilde{\theta}\right)-\sin\left(\frac{3}{2}\tilde{\theta}\right)\right)\\
U_{3}^{(B)}\left(r,\tilde{\theta},X_3\right) &= r^{\frac{3}{2}}\left(2\cos\left(\frac{1}{2}\tilde{\theta}\right)-3.066666\cos\left(\frac{3}{2}\tilde{\theta}\right)\right)
\end{aligned}
\tag{B.4}
$$

$$
\begin{aligned}
\varepsilon_{11}^{(B)}\left(r,\tilde{\theta},X_3\right) &= r^{-\frac{1}{2}}\left(1-X_3\right)\left(0.3\cos\left(\frac{1}{2}\tilde{\theta}\right)+0.5\cos\left(\frac{5}{2}\tilde{\theta}\right)\right)\\
\varepsilon_{22}^{(B)}\left(r,\tilde{\theta},X_3\right) &= r^{-\frac{1}{2}}\left(1-X_3\right)\left(1.3\cos\left(\frac{1}{2}\tilde{\theta}\right)-0.5\cos\left(\frac{5}{2}\tilde{\theta}\right)\right)\\
\varepsilon_{33}^{(B)}\left(r,\tilde{\theta},X_3\right) &= 0\\
\varepsilon_{12}^{(B)}\left(r,\tilde{\theta},X_3\right) &= r^{-\frac{1}{2}}\left(1-X_3\right)\left(-0.5\sin\left(\frac{1}{2}\tilde{\theta}\right)+0.5\sin\left(\frac{5}{2}\tilde{\theta}\right)\right)
\end{aligned}
\tag{B.5}
$$

$$\varepsilon_{13}^{(B)}\left(r,\tilde{\theta},X_3\right) = r^{\frac{1}{2}}\left(-2.6\cos\left(\frac{1}{2}\tilde{\theta}\right)+\cos\left(\frac{3}{2}\tilde{\theta}\right)\right)$$
$$\varepsilon_{23}^{(B)}\left(r,\tilde{\theta},X_3\right) = r^{\frac{1}{2}}\left(\sin\left(\frac{1}{2}\tilde{\theta}\right)+\sin\left(\frac{3}{2}\tilde{\theta}\right)\right)$$

and

$$\begin{aligned}
\sigma_{11}^{(B)}\left(r,\tilde{\theta},X_3\right) &= r^{-\frac{1}{2}}(1-X_3)\left(1.153845\cos\left(\frac{1}{2}\tilde{\theta}\right)+0.384615\cos\left(\frac{5}{2}\tilde{\theta}\right)\right)\\
\sigma_{22}^{(B)}\left(r,\tilde{\theta},X_3\right) &= r^{-\frac{1}{2}}(1-X_3)\left(1.923075\cos\left(\frac{1}{2}\tilde{\theta}\right)-0.384615\cos\left(\frac{5}{2}\tilde{\theta}\right)\right)\\
\sigma_{33}^{(B)}\left(r,\tilde{\theta},X_3\right) &= r^{-\frac{1}{2}}(1-X_3)\left(0.923076\cos\left(\frac{1}{2}\tilde{\theta}\right)\right)\\
\sigma_{12}^{(B)}\left(r,\tilde{\theta},X_3\right) &= r^{-\frac{1}{2}}(1-X_3)\left(-0.384615\sin\left(\frac{1}{2}\tilde{\theta}\right)+0.384615\sin\left(\frac{5}{2}\tilde{\theta}\right)\right)\\
\sigma_{13}^{(B)}\left(r,\tilde{\theta},X_3\right) &= r^{\frac{1}{2}}\left(-2\cos\left(\frac{1}{2}\tilde{\theta}\right)+0.76923\cos\left(\frac{3}{2}\tilde{\theta}\right)\right)\\
\sigma_{23}^{(B)}\left(r,\tilde{\theta},X_3\right) &= r^{\frac{1}{2}}\left(0.76923\sin\left(\frac{1}{2}\tilde{\theta}\right)+0.76923\sin\left(\frac{3}{2}\tilde{\theta}\right)\right)
\end{aligned} \tag{B.6}$$

B. 3. Displacements, strains and stresses for example problem (C)

$$\begin{aligned}
U_1^{(C)}\left(r,\tilde{\theta},X_3\right) &= r^{\frac{1}{2}}(1-X_3+X_3^2)\left(2.6\cos\left(\frac{1}{2}\tilde{\theta}\right)-\cos\left(\frac{3}{2}\tilde{\theta}\right)\right)\\
&\quad +r^{\frac{5}{2}}\left(-1.22222\cos\left(\frac{1}{2}\tilde{\theta}\right)+\cos\left(\frac{3}{2}\tilde{\theta}\right)-0.62400\cos\left(\frac{5}{2}\tilde{\theta}\right)\right)\\
U_2^{(C)}\left(r,\tilde{\theta},X_3\right) &= r^{\frac{1}{2}}(1-X_3+X_3^2)\left(4.6\sin\left(\frac{1}{2}\tilde{\theta}\right)-\sin\left(\frac{3}{2}\tilde{\theta}\right)\right)\\
&\quad +r^{\frac{5}{2}}\left(0.55555\sin\left(\frac{1}{2}\tilde{\theta}\right)+\sin\left(\frac{3}{2}\tilde{\theta}\right)-0.62400\sin\left(\frac{5}{2}\tilde{\theta}\right)\right)\\
U_3^{(C)}\left(r,\tilde{\theta},X_3\right) &= r^{\frac{3}{2}}(1-2X_3)\left(2\cos\left(\frac{1}{2}\tilde{\theta}\right)-3.066666\cos\left(\frac{3}{2}\tilde{\theta}\right)\right)
\end{aligned} \tag{B.7}$$

$$\begin{aligned}
\varepsilon_{11}^{(C)}\left(r,\tilde{\theta},X_3\right) &= r^{-\frac{1}{2}}(1-X_3+X_3^2)\left(0.3\cos\left(\frac{1}{2}\tilde{\theta}\right)+0.5\cos\left(\frac{5}{2}\tilde{\theta}\right)\right)\\
&\quad +r^{\frac{3}{2}}\left(0.66666\cos\left(\frac{1}{2}\tilde{\theta}\right)-2.78222\cos\left(\frac{3}{2}\tilde{\theta}\right)+0.5\cos\left(\frac{5}{2}\tilde{\theta}\right)\right)\\
\varepsilon_{22}^{(C)}\left(r,\tilde{\theta},X_3\right) &= r^{-\frac{1}{2}}(1-X_3+X_3^2)\left(1.3\cos\left(\frac{1}{2}\tilde{\theta}\right)-0.5\cos\left(\frac{5}{2}\tilde{\theta}\right)\right)\\
&\quad +r^{\frac{3}{2}}\left(2.23333\cos\left(\frac{1}{2}\tilde{\theta}\right)-1.71555\cos\left(\frac{3}{2}\tilde{\theta}\right)-0.5\cos\left(\frac{5}{2}\tilde{\theta}\right)\right)
\end{aligned}$$

$$\begin{aligned}
\varepsilon_{33}^{(C)}\left(r,\tilde{\theta},X_3\right) &= r^{\frac{3}{2}}\left(-4\cos\left(\frac{1}{2}\tilde{\theta}\right)+6.13333\cos\left(\frac{3}{2}\tilde{\theta}\right)\right)\\
\varepsilon_{12}^{(C)}\left(r,\tilde{\theta},X_3\right) &= r^{-\frac{1}{2}}\left(1-X_3+X_3^2\right)\left(-0.5\sin\left(\frac{1}{2}\tilde{\theta}\right)+0.5\sin\left(\frac{5}{2}\tilde{\theta}\right)\right)\\
&\quad +r^{\frac{3}{2}}\left(-1.03333\sin\left(\frac{1}{2}\tilde{\theta}\right)-0.53333\sin\left(\frac{3}{2}\tilde{\theta}\right)+0.5\sin\left(\frac{5}{2}\tilde{\theta}\right)\right)\\
\varepsilon_{13}^{(C)}\left(r,\tilde{\theta},X_3\right) &= r^{\frac{1}{2}}\left(1-2X_3\right)\left(-2.6\cos\left(\frac{1}{2}\tilde{\theta}\right)+\cos\left(\frac{3}{2}\tilde{\theta}\right)\right)\\
\varepsilon_{23}^{(C)}\left(r,\tilde{\theta},X_3\right) &= r^{\frac{1}{2}}\left(1-2X_3\right)\left(\sin\left(\frac{1}{2}\tilde{\theta}\right)+\sin\left(\frac{3}{2}\tilde{\theta}\right)\right)
\end{aligned}\tag{B.8}$$

and

$$\begin{aligned}
\sigma_{11}^{(C)}\left(r,\tilde{\theta},X_3\right) &= r^{-\frac{1}{2}}\left(1-X_3+X_3^2\right)\left(1.153845\cos\left(\frac{1}{2}\tilde{\theta}\right)+0.384615\cos\left(\frac{5}{2}\tilde{\theta}\right)\right)\\
&\quad +r^{\frac{3}{2}}\left(-0.79487\cos\left(\frac{1}{2}\tilde{\theta}\right)-1.19658\cos\left(\frac{3}{2}\tilde{\theta}\right)+0.384615\cos\left(\frac{5}{2}\tilde{\theta}\right)\right)\\
\sigma_{22}^{(C)}\left(r,\tilde{\theta},X_3\right) &= r^{-\frac{1}{2}}\left(1-X_3+X_3^2\right)\left(1.923075\cos\left(\frac{1}{2}\tilde{\theta}\right)-0.384615\cos\left(\frac{5}{2}\tilde{\theta}\right)\right)\\
&\quad +r^{\frac{3}{2}}\left(0.79487\cos\left(\frac{1}{2}\tilde{\theta}\right)-0.37607\cos\left(\frac{3}{2}\tilde{\theta}\right)-0.384615\cos\left(\frac{5}{2}\tilde{\theta}\right)\right)\\
\sigma_{33}^{(C)}\left(r,\tilde{\theta},X_3\right) &= r^{-\frac{1}{2}}\left(1-X_3+X_3^2\right)\left(0.923076\cos\left(\frac{1}{2}\tilde{\theta}\right)\right)+r^{\frac{3}{2}}\left(-4\cos\left(\frac{1}{2}\tilde{\theta}\right)+5.66153\cos\left(\frac{3}{2}\tilde{\theta}\right)\right)
\end{aligned}$$

$$\begin{aligned}
\sigma_{12}^{(C)}\left(r,\tilde{\theta},X_3\right) &= r^{-\frac{1}{2}}\left(1-X_3+X_3^2\right)\left(-0.384615\sin\left(\frac{1}{2}\tilde{\theta}\right)+0.384615\sin\left(\frac{5}{2}\tilde{\theta}\right)\right)\\
&\quad +r^{\frac{3}{2}}\left(0.79487\sin\left(\frac{1}{2}\tilde{\theta}\right)-0.41026\sin\left(\frac{3}{2}\tilde{\theta}\right)+0.384615\sin\left(\frac{5}{2}\tilde{\theta}\right)\right)\\
\sigma_{13}^{(C)}\left(r,\tilde{\theta},X_3\right) &= r^{\frac{1}{2}}\left(1-2X_3\right)\left(-2\cos\left(\frac{1}{2}\tilde{\theta}\right)+0.76923\cos\left(\frac{3}{2}\tilde{\theta}\right)\right)\\
\sigma_{23}^{(C)}\left(r,\tilde{\theta},X_3\right) &= r^{\frac{1}{2}}\left(1-2X_3\right)\left(0.76923\sin\left(\frac{1}{2}\tilde{\theta}\right)+0.76923\sin\left(\frac{3}{2}\tilde{\theta}\right)\right)
\end{aligned}\tag{B.9}$$

B. 4. Displacements, strains and stresses for example problem (D)

$$\begin{aligned}
U_1^{(D)}\left(r,\tilde{\theta},X_3\right) &= r^{\frac{1}{2}}\left(-3.15385\cos\left(\frac{1}{2}\tilde{\theta}\right)+0.384615\cos\left(\frac{3}{2}\tilde{\theta}\right)\right)\\
U_2^{(D)}\left(r,\tilde{\theta},X_3\right) &= r^{\frac{1}{2}}\left(0.384615\sin\left(\frac{1}{2}\tilde{\theta}\right)+0.384615\sin\left(\frac{3}{2}\tilde{\theta}\right)\right)\\
U_3^{(D)}\left(r,\tilde{\theta},X_3\right) &= 0
\end{aligned}\tag{B.10}$$

$$
\begin{aligned}
\varepsilon_{11}^{(D)}\left(r,\tilde{\theta},X_3\right) &= r^{-\frac{1}{2}}\left(-1.19231\cos\left(\frac{1}{2}\tilde{\theta}\right)-0.19231\cos\left(\frac{5}{2}\tilde{\theta}\right)\right)\\
\varepsilon_{22}^{(D)}\left(r,\tilde{\theta},X_3\right) &= r^{-\frac{1}{2}}\left(0.57692\cos\left(\frac{1}{2}\tilde{\theta}\right)+0.19231\cos\left(\frac{5}{2}\tilde{\theta}\right)\right)\\
\varepsilon_{33}^{(D)}\left(r,\tilde{\theta},X_3\right) &= 0\\
\varepsilon_{12}^{(D)}\left(r,\tilde{\theta},X_3\right) &= r^{-\frac{1}{2}}\left(-0.88462\sin\left(\frac{1}{2}\tilde{\theta}\right)-0.19231\sin\left(\frac{5}{2}\tilde{\theta}\right)\right)\\
\varepsilon_{13}^{(D)}\left(r,\tilde{\theta},X_3\right) &= 0\\
\varepsilon_{23}^{(D)}\left(r,\tilde{\theta},X_3\right) &= 0
\end{aligned}
\tag{B.11}
$$

and

$$
\begin{aligned}
\sigma_{11}^{(D)}\left(r,\tilde{\theta},X_3\right) &= r^{-\frac{1}{2}}\left(-1.27219\cos\left(\frac{1}{2}\tilde{\theta}\right)-0.14793\cos\left(\frac{5}{2}\tilde{\theta}\right)\right)\\
\sigma_{22}^{(D)}\left(r,\tilde{\theta},X_3\right) &= r^{-\frac{1}{2}}\left(0.08876\cos\left(\frac{1}{2}\tilde{\theta}\right)+0.14793\cos\left(\frac{5}{2}\tilde{\theta}\right)\right)\\
\sigma_{33}^{(D)}\left(r,\tilde{\theta},X_3\right) &= r^{-\frac{1}{2}}\left(-0.35502\cos\left(\frac{1}{2}\tilde{\theta}\right)\right)\\
\sigma_{12}^{(D)}\left(r,\tilde{\theta},X_3\right) &= r^{-\frac{1}{2}}\left(-0.68047\sin\left(\frac{1}{2}\tilde{\theta}\right)-0.14793\sin\left(\frac{5}{2}\tilde{\theta}\right)\right)\\
\sigma_{13}^{(D)}\left(r,\tilde{\theta},X_3\right) &= 0\\
\sigma_{23}^{(D)}\left(r,\tilde{\theta},X_3\right) &= 0
\end{aligned}
\tag{B.12}
$$

B. 5. Displacements, strains and stresses for example problem (E)

$$
\begin{aligned}
U_{1}^{(E)}\left(r,\tilde{\theta},X_3\right) &= r^{\frac{1}{2}}(1-X_3)\left(-3.15385\cos\left(\frac{1}{2}\tilde{\theta}\right)+0.384615\cos\left(\frac{3}{2}\tilde{\theta}\right)\right)\\
U_{2}^{(E)}\left(r,\tilde{\theta},X_3\right) &= r^{\frac{1}{2}}(1-X_3)\left(0.384615\sin\left(\frac{1}{2}\tilde{\theta}\right)+0.384615\sin\left(\frac{3}{2}\tilde{\theta}\right)\right)\\
U_{3}^{(E)}\left(r,\tilde{\theta},X_3\right) &= r^{\frac{3}{2}}\left(-0.76923\cos\left(\frac{1}{2}\tilde{\theta}\right)\right)
\end{aligned}
\tag{B.13}
$$

$$
\begin{aligned}
\varepsilon_{11}^{(E)}\left(r,\tilde{\theta},X_3\right) &= r^{-\frac{1}{2}}(1-X_3)\left(-1.19231\cos\left(\frac{1}{2}\tilde{\theta}\right)-0.19231\cos\left(\frac{5}{2}\tilde{\theta}\right)\right)\\
\varepsilon_{22}^{(E)}\left(r,\tilde{\theta},X_3\right) &= r^{-\frac{1}{2}}(1-X_3)\left(0.57692\cos\left(\frac{1}{2}\tilde{\theta}\right)+0.19231\cos\left(\frac{5}{2}\tilde{\theta}\right)\right)\\
\varepsilon_{33}^{(E)}\left(r,\tilde{\theta},X_3\right) &= 0\\
\varepsilon_{12}^{(E)}\left(r,\tilde{\theta},X_3\right) &= r^{-\frac{1}{2}}(1-X_3)\left(-0.88462\sin\left(\frac{1}{2}\tilde{\theta}\right)-0.19231\sin\left(\frac{5}{2}\tilde{\theta}\right)\right)
\end{aligned}
\tag{B.14}
$$

$$
\begin{aligned}
\varepsilon_{13}^{(E)}\left(r,\tilde{\theta},X_3\right) &= r^{\frac{1}{2}}\left(1.19231\cos\left(\frac{1}{2}\tilde{\theta}\right)-0.38462\cos\left(\frac{3}{2}\tilde{\theta}\right)\right)\\
\varepsilon_{23}^{(E)}\left(r,\tilde{\theta},X_3\right) &= r^{\frac{1}{2}}\left(-0.57692\sin\left(\frac{1}{2}\tilde{\theta}\right)-0.38462\sin\left(\frac{3}{2}\tilde{\theta}\right)\right)
\end{aligned}
$$

and

$$
\begin{aligned}
\sigma_{11}^{(E)}\left(r,\tilde{\theta},X_3\right) &= r^{-\frac{1}{2}}\left(1-X_3\right)\left(-1.27219\cos\left(\frac{1}{2}\tilde{\theta}\right)-0.14793\cos\left(\frac{5}{2}\tilde{\theta}\right)\right)\\
\sigma_{22}^{(E)}\left(r,\tilde{\theta},X_3\right) &= r^{-\frac{1}{2}}\left(1-X_3\right)\left(0.08876\cos\left(\frac{1}{2}\tilde{\theta}\right)+0.14793\cos\left(\frac{5}{2}\tilde{\theta}\right)\right)\\
\sigma_{33}^{(E)}\left(r,\tilde{\theta},X_3\right) &= r^{-\frac{1}{2}}\left(1-X_3\right)\left(-0.35502\cos\left(\frac{1}{2}\tilde{\theta}\right)\right) \qquad\qquad \text{(B.15)}\\
\sigma_{12}^{(E)}\left(r,\tilde{\theta},X_3\right) &= r^{-\frac{1}{2}}\left(1-X_3\right)\left(-0.68047\sin\left(\frac{1}{2}\tilde{\theta}\right)-0.14793\sin\left(\frac{5}{2}\tilde{\theta}\right)\right)
\end{aligned}
$$

$$
\begin{aligned}
\sigma_{13}^{(E)}\left(r,\tilde{\theta},X_3\right) &= r^{\frac{1}{2}}\left(0.91716\cos\left(\frac{1}{2}\tilde{\theta}\right)-0.29586\cos\left(\frac{3}{2}\tilde{\theta}\right)\right)\\
\sigma_{23}^{(E)}\left(r,\tilde{\theta},X_3\right) &= r^{\frac{1}{2}}\left(-0.44379\sin\left(\frac{1}{2}\tilde{\theta}\right)-0.29586\sin\left(\frac{3}{2}\tilde{\theta}\right)\right)
\end{aligned}
$$

B. 6. Displacements, strains and stresses for example problem (F)

$$
\begin{aligned}
U_1^{(F)}\left(r,\tilde{\theta},X_3\right) &= r^{\frac{1}{2}}\left(1-X_3+X_3^2\right)\left(-3.15385\cos\left(\frac{1}{2}\tilde{\theta}\right)+0.384615\cos\left(\frac{3}{2}\tilde{\theta}\right)\right)\\
&\quad +r^{\frac{5}{2}}\left(0.65772\cos\left(\frac{1}{2}\tilde{\theta}\right)-0.38462\cos\left(\frac{3}{2}\tilde{\theta}\right)-0.13715\cos\left(\frac{5}{2}\tilde{\theta}\right)\right)\\
U_2^{(F)}\left(r,\tilde{\theta},X_3\right) &= r^{\frac{1}{2}}\left(1-X_3+X_3^2\right)\left(0.384615\sin\left(\frac{1}{2}\tilde{\theta}\right)+0.384615\sin\left(\frac{3}{2}\tilde{\theta}\right)\right) \qquad \text{(B.16)}\\
&\quad +r^{\frac{5}{2}}\left(-0.24747\sin\left(\frac{1}{2}\tilde{\theta}\right)-0.38462\sin\left(\frac{3}{2}\tilde{\theta}\right)-0.13715\sin\left(\frac{5}{2}\tilde{\theta}\right)\right)\\
U_3^{(F)}\left(r,\tilde{\theta},X_3\right) &= r^{\frac{3}{2}}\left(1-2X_3\right)\left(-0.76923\cos\left(\frac{1}{2}\tilde{\theta}\right)\right)
\end{aligned}
$$

$$
\begin{aligned}
\varepsilon_{11}^{(F)}\left(r,\tilde{\theta},X_3\right) &= r^{-\frac{1}{2}}\left(1-X_3+X_3^2\right)\left(-1.19231\cos\left(\frac{1}{2}\tilde{\theta}\right)-0.19231\cos\left(\frac{5}{2}\tilde{\theta}\right)\right)\\
&\quad +r^{\frac{3}{2}}\left(0.21735\cos\left(\frac{1}{2}\tilde{\theta}\right)+0.31485\cos\left(\frac{3}{2}\tilde{\theta}\right)-0.19231\cos\left(\frac{5}{2}\tilde{\theta}\right)\right)\\
\varepsilon_{22}^{(F)}\left(r,\tilde{\theta},X_3\right) &= r^{-\frac{1}{2}}\left(1-X_3+X_3^2\right)\left(0.57692\cos\left(\frac{1}{2}\tilde{\theta}\right)+0.19231\cos\left(\frac{5}{2}\tilde{\theta}\right)\right)\\
&\quad +r^{\frac{3}{2}}\left(-1.14043\cos\left(\frac{1}{2}\tilde{\theta}\right)-0.09541\cos\left(\frac{3}{2}\tilde{\theta}\right)+0.19231\cos\left(\frac{5}{2}\tilde{\theta}\right)\right)
\end{aligned}
$$

$$\begin{aligned}
\varepsilon_{33}^{(F)}\left(r,\tilde{\theta},X_3\right) &= r^{\frac{3}{2}}\left(1.5385\cos\left(\frac{1}{2}\tilde{\theta}\right)\right) \qquad \text{(B.17)}\\
\varepsilon_{12}^{(F)}\left(r,\tilde{\theta},X_3\right) &= r^{-\frac{1}{2}}\left(1-X_3+X_3^2\right)\left(-0.88462\sin\left(\frac{1}{2}\tilde{\theta}\right)-0.19231\sin\left(\frac{5}{2}\tilde{\theta}\right)\right)\\
&\quad +r^{\frac{3}{2}}\left(0.67889\sin\left(\frac{1}{2}\tilde{\theta}\right)+0.20513\sin\left(\frac{3}{2}\tilde{\theta}\right)-0.19231\sin\left(\frac{5}{2}\tilde{\theta}\right)\right)\\
\varepsilon_{13}^{(F)}\left(r,\tilde{\theta},X_3\right) &= r^{\frac{1}{2}}\left(1-2X_3\right)\left(1.19231\cos\left(\frac{1}{2}\tilde{\theta}\right)-0.38462\cos\left(\frac{3}{2}\tilde{\theta}\right)\right)\\
\varepsilon_{23}^{(F)}\left(r,\tilde{\theta},X_3\right) &= r^{\frac{1}{2}}\left(1-2X_3\right)\left(-0.57692\sin\left(\frac{1}{2}\tilde{\theta}\right)-0.38462\sin\left(\frac{3}{2}\tilde{\theta}\right)\right)
\end{aligned}$$

and

$$\begin{aligned}
\sigma_{11}^{(F)}\left(r,\tilde{\theta},X_3\right) &= r^{-\frac{1}{2}}\left(1-X_3+X_3^2\right)\left(-1.27219\cos\left(\frac{1}{2}\tilde{\theta}\right)-0.14793\cos\left(\frac{5}{2}\tilde{\theta}\right)\right)\\
&\quad +r^{\frac{3}{2}}\left(0.52222\cos\left(\frac{1}{2}\tilde{\theta}\right)+0.36879\cos\left(\frac{3}{2}\tilde{\theta}\right)-0.14793\cos\left(\frac{5}{2}\tilde{\theta}\right)\right)
\end{aligned}$$

$$\begin{aligned}
\sigma_{22}^{(F)}\left(r,\tilde{\theta},X_3\right) &= r^{-\frac{1}{2}}\left(1-X_3+X_3^2\right)\left(0.08876\cos\left(\frac{1}{2}\tilde{\theta}\right)+0.14793\cos\left(\frac{5}{2}\tilde{\theta}\right)\right)\\
&\quad +r^{\frac{3}{2}}\left(-0.52222\cos\left(\frac{1}{2}\tilde{\theta}\right)+0.05321\cos\left(\frac{3}{2}\tilde{\theta}\right)+0.14793\cos\left(\frac{5}{2}\tilde{\theta}\right)\right)
\end{aligned}$$

$$\begin{aligned}
\sigma_{33}^{(F)}\left(r,\tilde{\theta},X_3\right) &= r^{-\frac{1}{2}}\left(1-X_3+X_3^2\right)\left(-0.35502\cos\left(\frac{1}{2}\tilde{\theta}\right)\right)\\
&\quad +r^{\frac{3}{2}}\left(1.53846\cos\left(\frac{1}{2}\tilde{\theta}\right)+0.12659\cos\left(\frac{3}{2}\tilde{\theta}\right)\right)\\
\sigma_{12}^{(F)}\left(r,\tilde{\theta},X_3\right) &= r^{-\frac{1}{2}}\left(1-X_3+X_3^2\right)\left(-0.68047\sin\left(\frac{1}{2}\tilde{\theta}\right)-0.14793\sin\left(\frac{5}{2}\tilde{\theta}\right)\right) \qquad \text{(B.18)}\\
&\quad +r^{\frac{3}{2}}\left(0.52222\sin\left(\frac{1}{2}\tilde{\theta}\right)+0.15779\sin\left(\frac{3}{2}\tilde{\theta}\right)-0.14793\sin\left(\frac{5}{2}\tilde{\theta}\right)\right)\\
\sigma_{13}^{(F)}\left(r,\tilde{\theta},X_3\right) &= r^{\frac{1}{2}}\left(1-2X_3\right)\left(0.91716\cos\left(\frac{1}{2}\tilde{\theta}\right)-0.29586\cos\left(\frac{3}{2}\tilde{\theta}\right)\right)\\
\sigma_{23}^{(F)}\left(r,\tilde{\theta},X_3\right) &= r^{\frac{1}{2}}\left(1-2X_3\right)\left(-0.44379\sin\left(\frac{1}{2}\tilde{\theta}\right)-0.29586\sin\left(\frac{3}{2}\tilde{\theta}\right)\right)
\end{aligned}$$

Appendix C: Numerical and exact values of $J_{X_1}^{\text{path}}$, $J_{X_1}^{\text{area}}$ and J_{X_1} computed at $X_3 = -0.2$ for example problems (A)–(F)

Table C1. Numerical and exact values of $J_{X_1}^{\text{path}(A)}$, $J_{X_1}^{\text{area}(A)}$ and $J_{X_1}^{(A)}$ computed at $X_3 = -0.2$.

	$J_{X_1}^{\text{path}}$			$J_{X_1}^{\text{area}}$		J_{X_1}		
	Exact	numeric	% Error	Exact	numeric	Exact	numeric	% Error
$R=0.85$	13.53300	13.54290	−0.07315	0	−0.00002	13.53300	13.54292	−0.07332
$R=0.80$	13.53300	13.54487	−0.08770	0	−0.00010	13.53300	13.54496	−0.08842
$R=0.75$	13.53300	13.52752	0.04047	0	−0.00007	13.53300	13.52759	0.03995
$R=0.70$	13.53300	13.52562	0.05453	0	0.00002	13.53300	13.52560	0.05470
$R=0.65$	13.53300	13.52719	0.04289	0	0.00011	13.53300	13.52709	0.04368
$R=0.60$	13.53300	13.53765	−0.03436	0	0.00013	13.53300	13.53752	−0.03340
$R=0.55$	13.53300	13.53909	−0.04503	0	0.00017	13.53300	13.53892	−0.04375
$R=0.50$	13.53300	13.55302	−0.14796	0	0.00010	13.53300	13.55393	−0.15467
$R=0.45$	13.53300	13.53890	−0.04357	0	−0.00005	13.53300	13.53895	−0.04396
$R=0.40$	13.53300	13.53269	0.00228	0	−0.00019	13.53300	13.53288	0.00085
$R=0.35$	13.53300	13.52421	0.06498	0	−0.00004	13.53300	13.52425	0.06468
$R=0.30$	13.53300	13.52422	0.06489	0	−0.00002	13.53300	13.52424	0.06473
$R=0.25$	13.53300	13.52468	0.06146	0	0.00006	13.53300	13.52462	0.06190
$R=0.20$	13.53300	13.53017	0.02094	0	0.00002	13.53300	13.53014	0.02109
$R=0.15$	13.53300	13.53003	0.02194	0	0.00006	13.53300	13.52997	0.02238
$R=0.10$	13.53300	13.51938	0.10060	0	−0.00001	13.53300	13.51939	0.10054
$R=0.05$	13.53300	13.48695	0.34030	0	0.00000	13.53300	13.48695	0.34031

Table C2. Numerical and exact values of $J_{X_1}^{\text{path}(B)}$, $J_{X_1}^{\text{area}(B)}$ and $J_{X_1}^{(B)}$ computed at $X_3 = -0.2$.

	$J_{X_1}^{\text{path}}$			$J_{X_1}^{\text{area}}$			J_{X_1}		
	Exact	Numeric	% Error	Exact	Numeric	% Error	Exact	Numeric	% Error
$R=0.85$	25.77311	25.78427	−0.04331	6.28559	6.28607	−0.00751	19.48752	19.49821	−0.05485
$R=0.80$	25.05538	25.07063	−0.06085	5.56786	5.56564	0.04000	19.48752	19.50499	−0.08967
$R=0.75$	24.38115	24.37309	0.03303	4.89363	4.89316	0.00949	19.48752	19.47993	0.03894
$R=0.70$	23.75041	23.73566	0.06211	4.26289	4.26294	−0.00115	19.48752	19.47272	0.07595
$R=0.65$	23.16318	23.15176	0.04928	3.67566	3.67440	0.03414	19.48752	19.47736	0.05213
$R=0.60$	22.61944	22.62337	−0.01736	3.13192	3.13211	−0.00602	19.48752	19.49126	−0.01918
$R=0.55$	22.11920	22.12737	−0.03693	2.63168	2.63195	−0.01021	19.48752	19.49542	−0.04054
$R=0.50$	21.66246	21.69289	−0.14046	2.17495	2.17436	0.02679	19.48752	19.51853	−0.15913
$R=0.45$	21.24922	21.25777	−0.04022	1.76171	1.76074	0.05482	19.48752	19.49703	−0.04881
$R=0.40$	20.87948	20.87820	0.00616	1.39197	1.39086	0.07940	19.48752	19.48734	0.00093
$R=0.35$	20.55324	20.53975	0.06564	1.06572	1.06468	0.09764	19.48752	19.47507	0.06389
$R=0.30$	20.27050	20.25741	0.06457	0.78298	0.78270	0.03540	19.48752	19.47471	0.06574
$R=0.25$	20.03126	20.01808	0.06578	0.54374	0.54379	−0.00951	19.48752	19.47429	0.06788
$R=0.20$	19.83551	19.83177	0.01887	0.34799	0.34777	0.06491	19.48752	19.48400	0.01804

Table C2. Continued.

	$J_{X_1}^{\text{path}}$			$J_{X_1}^{\text{area}}$			J_{X_1}		
	Exact	Numeric	% Error	Exact	Numeric	% Error	Exact	Numeric	% Error
$R=0.15$	19.68326	19.67844	0.02452	0.19575	0.19545	0.15129	19.48752	19.48299	0.02324
$R=0.10$	19.57452	19.55443	0.10261	0.08700	0.08679	0.24407	19.48752	19.46765	0.10198
$R=0.05$	19.50927	19.44247	0.34241	0.02175	0.02167	0.35050	19.48752	19.42079	0.34240

Table C3. Numerical and exact values of $J_{X_1}^{\text{path}(C)}$, $J_{X_1}^{\text{area}(C)}$ and $J_{X_1}^{(C)}$ computed at $X_3=-0.2$.

	$J_{X_1}^{\text{path}}$			$J_{X_1}^{\text{area}}$			J_{X_1}		
	Exact	Numeric	% Error	Exact	Numeric	% Error	Exact	Numeric	% Error
$R=0.85$	37.34620	37.32753	0.04999	16.53786	16.53933	−0.00886	20.80834	20.78820	0.09677
$R=0.80$	36.60787	36.60013	0.02114	15.79953	15.79001	0.06023	20.80834	20.81012	−0.00855
$R=0.75$	35.64419	35.62643	0.04982	14.83585	14.82871	0.04811	20.80834	20.79772	0.05104
$R=0.70$	34.50581	34.48207	0.06881	13.69747	13.69433	0.02293	20.80834	20.78774	0.09900
$R=0.65$	33.24010	33.22225	0.05369	12.43176	12.42262	0.07356	20.80834	20.79964	0.04183
$R=0.60$	31.89117	31.88967	0.00470	11.08283	11.08173	0.00993	20.80834	20.80794	0.00192
$R=0.55$	30.49986	30.50357	−0.01215	9.69152	9.69116	0.00371	20.80834	20.81240	−0.01954
$R=0.50$	29.10374	29.13655	−0.11273	8.29541	8.29329	0.02553	20.80834	20.84327	−0.16786
$R=0.45$	27.73713	27.74181	−0.01687	6.92879	6.92689	0.02747	20.80834	20.81492	−0.03163
$R=0.40$	26.43105	26.43627	−0.01972	5.62272	5.61993	0.04960	20.80834	20.80634	0.00960
$R=0.35$	25.21329	25.19746	0.06280	4.40495	4.39910	0.13290	20.80834	20.79836	0.04796
$R=0.30$	24.10834	24.09450	0.05743	3.30000	3.29699	0.09138	20.80834	20.79751	0.05204
$R=0.25$	23.13744	23.12019	0.07459	2.32911	2.32697	0.09178	20.80834	20.79322	0.07267
$R=0.20$	22.31857	22.30964	0.04003	1.51023	1.50953	0.04639	20.80834	20.80011	0.03957
$R=0.15$	21.66642	21.65805	0.03864	0.85808	0.85739	0.08085	20.80834	20.80066	0.03690
$R=0.10$	21.19243	21.16952	0.10813	0.38409	0.38334	0.19662	20.80834	20.78618	0.10650
$R=0.05$	20.90477	20.83412	0.33798	0.09643	0.09588	0.57275	20.80834	20.73824	0.33689

Table C4. Numerical and exact values of $J_{X_1}^{\text{path}(D)}$, $J_{X_1}^{\text{area}(D)}$ and $J_{X_1}^{(D)}$ computed at $X_3=-0.2$.

	$J_{X_1}^{\text{path}}$			$J_{X_1}^{\text{area}}$		J_{X_1}		
	Exact	numeric	% Error	Exact	numeric	Exact	numeric	% Error
$R=0.85$	−3.60346	−3.60566	−0.06101	0	0.00005	−3.60346	−3.60571	−0.06245
$R=0.80$	−3.60346	−3.60541	−0.05415	0	0.00007	−3.60346	−3.60549	−0.05623
$R=0.75$	−3.60346	−3.60329	0.00473	0	0.00007	−3.60346	−3.60336	0.00281
$R=0.70$	−3.60346	−3.60176	0.04731	0	0.00004	−3.60346	−3.60180	0.04618
$R=0.65$	−3.60346	−3.60164	0.05065	0	0.00000	−3.60346	−3.60164	0.05054
$R=0.60$	−3.60346	−3.60349	−0.00071	0	−0.00003	−3.60346	−3.60346	0.00019
$R=0.55$	−3.60346	−3.60542	−0.05425	0	−0.00002	−3.60346	−3.60539	−0.05361
$R=0.50$	−3.60346	−3.60626	−0.07765	0	0.00001	−3.60346	−3.60627	−0.07787
$R=0.45$	−3.60346	−3.60525	−0.04962	0	0.00005	−3.60346	−3.60530	−0.05099

Table C4. Continued.

	$J_{X_1}^{\text{path}}$			$J_{X_1}^{\text{area}}$		J_{X_1}		
	Exact	numeric	% Error	Exact	numeric	Exact	numeric	% Error
$R=0.40$	−3.60346	−3.60275	0.01979	0	0.00005	−3.60346	−3.60280	0.01849
$R=0.35$	−3.60346	−3.60048	0.08272	0	0.00002	−3.60346	−3.60050	0.08216
$R=0.30$	−3.60346	−3.60158	0.05222	0	0.00000	−3.60346	−3.60158	0.05218
$R=0.25$	−3.60346	−3.60756	−0.11379	0	−0.00002	−3.60346	−3.60755	−0.11332
$R=0.20$	−3.60346	−3.60614	−0.07426	0	−0.00001	−3.60346	−3.60612	−0.07375
$R=0.15$	−3.60346	−3.60497	−0.04185	0	0.00000	−3.60346	−3.60497	−0.04190
$R=0.10$	−3.60346	−3.60554	−0.05756	0	0.00000	−3.60346	−3.60554	−0.05755
$R=0.05$	−3.60346	−3.60685	−0.09395	0	0.00000	−3.60346	−3.60685	−0.09394

Table C5. Numerical and analytical values of $J_{X_1}^{\text{path}(E)}$, $J_{X_1}^{\text{area}(E)}$ and $J_{X_1}^{(E)}$ computed at $X_3=-0.2$.

	$J_{X_1}^{\text{path}}$			$J_{X_1}^{\text{area}}$			J_{X_1}		
	Exact	Numeric	% Error	Exact	Numeric	% Error	Exact	Numeric	% Error
$R=0.85$	−4.16102	−4.16478	−0.09037	1.02797	1.02785	0.01135	−5.18899	−5.19263	−0.07022
$R=0.80$	−4.27840	−4.28200	−0.08420	0.91059	0.91073	−0.01564	−5.18899	−5.19273	−0.07217
$R=0.75$	−4.38866	−4.38847	0.00442	0.80032	0.80035	−0.00375	−5.18899	−5.18882	0.00317
$R=0.70$	−4.49182	−4.48897	0.06340	0.69717	0.69710	0.01054	−5.18899	−5.18606	0.05630
$R=0.65$	−4.58786	−4.58503	0.06166	0.60113	0.60106	0.01177	−5.18899	−5.18609	0.05588
$R=0.60$	−4.67678	−4.67684	−0.00125	0.51221	0.51197	0.04562	−5.18899	−5.18881	0.00338
$R=0.55$	−4.75859	−4.76133	−0.05762	0.43040	0.43013	0.06239	−5.18899	−5.19146	−0.04767
$R=0.50$	−4.83329	−4.83741	−0.08524	0.35570	0.35554	0.04352	−5.18899	−5.19295	−0.07641
$R=0.45$	−4.90087	−4.90361	−0.05588	0.28812	0.28813	−0.00339	−5.18899	−5.19173	−0.05297
$R=0.40$	−4.96134	−4.96052	0.01656	0.22765	0.22774	−0.03864	−5.18899	−5.18825	0.01414
$R=0.35$	−5.01469	−5.01054	0.08292	0.17429	0.17429	0.00285	−5.18899	−5.18482	0.08023
$R=0.30$	−5.06093	−5.05826	0.05292	0.12805	0.12800	0.03927	−5.18899	−5.18626	0.05259
$R=0.25$	−5.10006	−5.10595	−0.11542	0.08892	0.08882	0.12060	−5.18899	−5.19477	−0.11137
$R=0.20$	−5.13207	−5.13603	−0.07699	0.05691	0.05681	0.17794	−5.18899	−5.19284	−0.07419
$R=0.15$	−5.15697	−5.15919	−0.04295	0.03201	0.03194	0.23581	−5.18899	−5.19113	−0.04123
$R=0.10$	−5.17476	−5.17768	−0.05641	0.01423	0.01416	0.45926	−5.18899	−5.19184	−0.05500
$R=0.05$	−5.18543	−5.19029	−0.09377	0.00356	0.00352	1.17840	−5.18899	−5.19381	−0.09290

Table C6. Numerical and exact values of $J_{X_1}^{\text{path}(F)}$, $J_{X_1}^{\text{area}(F)}$ and $J_{X_1}^{(F)}$ computed at $X_3=-0.2$.

	$J_{X_1}^{\text{path}}$			$J_{X_1}^{\text{area}}$			J_{X_1}		
	Exact	Numeric	% Error	Exact	Numeric	% Error	Exact	Numeric	% Error
$R=0.85$	−4.16102	−4.16478	−0.09037	1.02797	1.02785	0.01135	−5.18899	−5.19263	−0.07022
$R=0.80$	−4.27840	−4.28200	−0.08420	0.91059	0.91073	−0.01564	−5.18899	−5.19273	−0.07217
$R=0.75$	−4.38866	−4.38847	0.00442	0.80032	0.80035	−0.00375	−5.18899	−5.18882	0.00317
$R=0.70$	−4.49182	−4.48897	0.06340	0.69717	0.69710	0.01054	−5.18899	−5.18606	0.05630

Table C6. Continued.

	$J_{X_1}^{\text{path}}$			$J_{X_1}^{\text{area}}$			J_{X_1}		
	Exact	Numeric	% Error	Exact	Numeric	% Error	Exact	Numeric	% Error
$R = 0.65$	−4.58786	−4.58503	0.06166	0.60113	0.60106	0.01177	−5.18899	−5.18609	0.05588
$R = 0.60$	−4.67678	−4.67684	−0.00125	0.51221	0.51197	0.04562	−5.18899	−5.18881	0.00338
$R = 0.55$	−4.75859	−4.76133	−0.05762	0.43040	0.43013	0.06239	−5.18899	−5.19146	−0.04767
$R = 0.50$	−4.83329	−4.83741	−0.08524	0.35570	0.35554	0.04352	−5.18899	−5.19295	−0.07641
$R = 0.45$	−4.90087	−4.90361	−0.05588	0.28812	0.28813	−0.00339	−5.18899	−5.19173	−0.05297
$R = 0.40$	−4.96134	−4.96052	0.01656	0.22765	0.22774	−0.03864	−5.18899	−5.18825	0.01414
$R = 0.35$	−5.01469	−5.01054	0.08292	0.17429	0.17429	0.00285	−5.18899	−5.18482	0.08023
$R = 0.30$	−5.06093	−5.05826	0.05292	0.12805	0.12800	0.03927	−5.18899	−5.18626	0.05259
$R = 0.25$	−5.10006	−5.10595	−0.11542	0.08892	0.08882	0.12060	−5.18899	−5.19477	−0.11137
$R = 0.20$	−5.13207	−5.13603	−0.07699	0.05691	0.05681	0.17794	−5.18899	−5.19284	−0.07419
$R = 0.15$	−5.15697	−5.15919	−0.04295	0.03201	0.03194	0.23581	−5.18899	−5.19113	−0.04123
$R = 0.10$	−5.17476	−5.17768	−0.05641	0.01423	0.01416	0.45926	−5.18899	−5.19184	−0.05500
$R = 0.05$	−5.18543	−5.19029	−0.09377	0.00356	0.00352	1.17840	−5.18899	−5.19381	−0.09290

References

Cherepanov, G. (1967). Crack propagation in continuous media. *Journal of Applied Mathematics and Mechanics* **31**(3), 503–512.

Chiarelli, M. and Frediani, A. (1993). A computation of the 3-dimensional J-integral for elastic-materials with a view to applications in fracture-mechanics. *Engineering Fracture Mechanics* **44**(5), 763–788.

Costabel, M. and Dauge, M. (1993). General edge asymptotics of solution of second order elliptic boundary value problems I & II. *Proceedings of the Royal Society of Edinburgh* **123A**, 109–184.

Costabel, M., Dauge, M. and Yosibash, Z. (2004). A quasidual function method for extracting edge stress intensity functions'. *SIAM Journal of Mathematical Analysis* **35**(5), 1177–1202.

Dauge, M. (1988). *Elliptic boundary value problems in corner domains - smoothness and asymptotics of solutions*. Lecture notes in Mathematics 1341, Springer-Verlag, Heidelberg.

Eriksson, K. (2000). A general expression for an area integral of a point-wise J for a curved crack front. *International Journal of Fracture* **106**, 65–80.

Gosz, M., Dolbow, J. and Moran, B. (1998). Domain integral formulation for stress intensity factor computation along curved three-dimensional interface cracks. *International Journal of Solids and Structures* **35**(15), 1763–1783.

Hartranft, R. and Sih, G. (1967). The use of eigenfunction expansions in the general solution of three-dimensional crack problems. *Journal of Mathematical Mechanics* **19**(2), 123–138.

Huber, O., Nickel, J. and Kuhn, G. (1993). On the decomposition of the J-integral for 3D crack problems. *International Journal of Fracture* **64**(4), 339–348.

Leblond, J. and Torlai, O. (1992). The stress-field near the front of an arbitrarily shaped crack in a 3-dimensional elastic body. *Journal of Elasticity* **29**(2), 97–131.

Omer, N., Yosibash, Z., Costabel, M. and Dauge, M. (2004). Edge flux intensity functions in polyhedral domains and their extraction by a quasidual function method. *International Journal of Fracture* **129**, 97–130.

Rice, J. (1968). A path independent integral and the approximate analysis of strain concentration by notches and cracks. *Journal of Applied Mechanics* **35**(2), 379–386.

Rigby, R. and Aliabadi, M. (1998). Decomposition of the mixed-mode J integral – revisited. *International Journal of Solids and Structures* **35**(17), 2073–2099.

Shih, C., Moran, B. and Nakamura, T. (1986). Energy-release rate along a 3-dimensional crack front in a thermally stressed body. *International Journal of Fracture* **30**(2), 79–102.

Szabó, B. A. and Babuška, I. (1991). *Finite Element Analysis*. New York: John Wiley & Sons.